The Meteoritical Society

Meteoritics & Planetary Science 52, Nr 5, 807–826 (2017)
doi: 10.1111/maps.12834

In search of the Earth-forming reservoir: Mineralogical, chemical, and isotopic characterizations of the ungrouped achondrite NWA 5363/NWA 5400 and selected chondrites

Christoph BURKHARDT[1,2,*], Nicolas DAUPHAS[1], Haolan TANG[1,3], Mario FISCHER-GÖDDE[2], Liping QIN[4], James H. CHEN[5], Surya S. ROUT[6], Andreas PACK[7], Philipp R. HECK[6], and Dimitri A. PAPANASTASSIOU[5,8]

[1]Origins Laboratory, Department of the Geophysical Sciences, The University of Chicago, Chicago, Illinois 60637, USA
[2]Institut für Planetologie, Westfälische Wilhelms-Universität Münster, Wilhelm-Klemm-Str 10, Münster D-48149, Germany
[3]Department of Earth, Planetary and Space Sciences, University of California, 595 Charles Young Drive East, Box 951567, Los Angeles, California 90095-1567, USA
[4]CAS Key Laboratory of Crust–Mantle Materials and Environments, School of Earth and Space Science, University of Science and Technology of China, 96 Jinzhai Rd, Hefei, Anhui 230026, PR China
[5]Jet Propulsion Laboratory, California Institute of Technology, 4800 Oak Grove Dr., Pasadena, California 91109, USA
[6]Robert A. Pritzker Center for Meteoritics and Polar Studies, The Field Museum, 1400 S Lake Shore Dr., Chicago, Illinois 60605, USA
[7]Geowissenschaftliches Zentrum, Abteilung Isotopengeologie, Goldschmidtstraße 3, Göttingen D-37077, Germany
[8]Division of Geological and Planetary Sciences, California Institute of Technology, Mail Code 170-25, 1200 E. California Blvd., Pasadena, California 91125, USA
[*]Corresponding author. E-mail: burkhardt@uni-muenster.de

(Received 08 July 2016; revision accepted 26 December 2016)

Abstract–High-precision isotope data of meteorites show that the long-standing notion of a "chondritic uniform reservoir" is not always applicable for describing the isotopic composition of the bulk Earth and other planetary bodies. To mitigate the effects of this "isotopic crisis" and to better understand the genetic relations of meteorites and the Earth-forming reservoir, we performed a comprehensive petrographic, elemental, and multi-isotopic (O, Ca, Ti, Cr, Ni, Mo, Ru, and W) study of the ungrouped achondrites NWA 5363 and NWA 5400, for both of which terrestrial O isotope signatures were previously reported. Also, we obtained isotope data for the chondrites Pillistfer (EL6), Allegan (H6), and Allende (CV3), and compiled available anomaly data for undifferentiated and differentiated meteorites. The chemical compositions of NWA 5363 and NWA 5400 are strikingly similar, except for fluid mobile elements tracing desert weathering. We show that NWA 5363 and NWA 5400 are paired samples from a primitive achondrite parent-body and interpret these rocks as restite assemblages after silicate melt extraction and siderophile element addition. Hafnium-tungsten chronology yields a model age of 2.2 ± 0.8 Myr after CAI, which probably dates both of these events within uncertainty. We confirm the terrestrial O isotope signature of NWA 5363/NWA 5400; however, the discovery of nucleosynthetic anomalies in Ca, Ti, Cr, Mo, and Ru reveals that the NWA5363/NWA 5400 parent-body is not the "missing link" that could explain the composition of the Earth by the mixing of known meteorites. Until this "missing link" or a direct sample of the terrestrial reservoir is identified, guidelines are provided of how to use chondrites for estimating the isotopic composition of the bulk Earth.

INTRODUCTION

The bulk chemical and isotopic compositions of a differentiated planet like the Earth cannot be determined directly. The composition of mantle rocks has to be supplemented with other proxy compositions, namely the composition of the Sun (which comprises 99.8% of the mass of the solar system) and the compositions of primitive undifferentiated meteorites that were never heated above the solidus temperature after their formation in the solar nebula (e.g., Palme and O'Neill 2014). The relative abundances of refractory elements in these chondritic meteorites are the same as those of the Sun and it is often assumed that chondrites represent the building blocks of the terrestrial planets. The introduction of the notion of a chondritic bulk planetary composition (Goldschmidt 1929; Russell 1941) boosted understanding of the structure, evolution, and inner workings of Earth and the other planets and still forms the backbone of geochemistry today (Palme and O'Neill 2014).

However, with ever-increasing precision in isotopic analyses, it has become clear in the last decade that known groups of chondrites, and in particular, the ones that are most often used to explain the chemical composition of the Earth (Allègre et al. 1995), display nucleosynthetic isotopic anomalies relative to terrestrial rocks (Dauphas et al. 2002, 2014a, 2014b; Andreasen and Sharma 2007; Trinquier et al. 2007, 2009; Regelous et al. 2008; Chen et al. 2010, 2011; Qin et al. 2010; Burkhardt et al. 2011, 2016; Gannoun et al., 2011; Moynier et al. 2012; Herwartz et al. 2014; Akram et al. 2015; Render et al. 2016). Under the assumption that the measured isotopic composition of the accessible Earth represents the composition of the bulk Earth, which seems reasonable at least for the lithophile elements that are not affected by radioactive decay or core partitioning (for siderophile elements, this is only true if the material accreted by the Earth did not change as a function of time [Dauphas et al. 2004; Dauphas 2017]), the nucleosynthetic anomalies thus showed that no known chondrite group nor any combination of known chondrite groups are viable building blocks for the Earth (Burkhardt et al. 2011, 2016).

The lack of a proper meteoritic proxy for the composition of Earth has important implications for our understanding of its origin and development. For example, using ordinary chondrites as proxy for the $^{142}Nd/^{144}Nd$ of the bulk Earth leads to incorrect interpretations of the ^{142}Nd rock record to determine accretion and differentiation time scales of the Earth (Burkhardt et al. 2011, 2016; Gannoun et al. 2011). Likewise, taking the Si isotope composition of enstatite, ordinary, or carbonaceous chondrites as representative of the bulk Earth may lead to wrong assumptions about the Earth's Mg/Si ratio and the amount of Si in the Earth's core (Dauphas et al. 2015).

If known chondrite types are not always good isotopic proxies for the planetary materials that formed Earth, are there any meteorites that are? The ungrouped (paired) primitive achondrites NWA 5363 and NWA 5400 are relatively oxidized (~IW-1; Gardner-Vandy et al. 2013), metal-bearing ultramafic rocks for which terrestrial O and Cr isotope compositions have been reported (Irving et al. 2009; Shukolyukov et al. 2010; Larouci et al. 2013). Thus, NWA 5363 and NWA 5400 may represent primitive samples of the elusive terrestrial reservoir. As part of our ongoing effort to better constrain the isotopic composition of the bulk Earth and the genetic relations of meteorites and the Earth-forming reservoir, we present here a comprehensive petrographic, elemental, and multi-isotopic (O, Ca, Ti, Cr, Ni, Mo, Ru, and W) study of the NWA 5363/NWA 5400 meteorites, as well as isotope data for the chondrites Pillistfer (EL6), Allegan (H6), and Allende (CV3) for quality control. Our results are discussed with respect to (1) the formation and differentiation history of the NWA 5363/NWA 5400 parent-body, (2) the relationship of NWA 5363/NWA 5400 to other known planetary materials, and (3) the nature of Earth-forming building blocks.

ANALYTICAL METHODS

Petrography

Several NWA 5363 rock slices of a few grams each and a single 34 g slice of NWA 5400 were purchased from meteorite dealers. Visual inspection of the slices indicates that both meteorites are affected by desert weathering, with NWA 5400 being more strongly altered than NWA 5363. For each meteorite, an epoxy-mounted 1″ thick section was prepared and polished using different grits of SiC paper and diamond paste. The sections were investigated using a Zeiss EVO 60 SEM equipped with an Oxford EDS (energy dispersive spectroscopy) system at the Field Museum of Natural History, Chicago. EDS maps of different elements were prepared for the whole surface of the sample to locate the distribution of different phases and estimate their abundance. Quantitative elemental composition of the phases was determined using the INCA analytical program provided by Oxford Instruments. A 20 kV electron beam was used to measure natural and synthetic standards prior to measuring the composition of the phases in the sample and the beam stability was monitored regularly.

Major and Trace Element Analysis

For major element, trace element, and isotopic analysis about 3–5 g pieces of NWA 5363, NWA 5400, Pillistfer (EL6; Field Museum, ME 2655 #1), Allegan (H6; Field Museum, ME 1433 #3.1), and Allende (CV3; Field Museum, ME 2639) were cleaned with abrasive paper, followed by ultrasonication in methanol, and subsequently crushed and powdered in an acid-cleaned agate mortar at the Origins Lab, Chicago. Care was taken to use the least altered sections available. To investigate the effects of desert weathering on the elemental and isotopic composition of the NWA meteorites, a severely altered part of NWA 5400 was also powdered (NWA 5400alt). Visual examination of the powdered samples confirms the grading of weathering, with the colors of the powders progressing from dark gray (NWA 5363) to brownish-yellow (NWA 5400) to yellow-reddish (NWA 5400alt). Bulk major and trace element analyses of the NWA 5363, NWA 5400, NWA 5400alt samples, as well as the Allende Smithsonian reference powder (USNM 3529; for quality control) were obtained on ~1 g aliquots of the powders at the SARM/CNRS Nancy, France by ICP-OES (Thermo Fisher ICap 6500), ICP-MS (Thermo Elemental X7), carbon-sulfur analyzer (Horiba EMIA320V2), and AAS (Varian 220FS), following the procedures laid out in Carignan et al. (2001).

Isotope Analysis

O Isotopes

About 0.15 g aliquots of the sample powders along with the BHVO-2 basalt standard were sent to the University of Göttingen, Germany, where their O isotope composition was analyzed by laser-fluorination gas-chromatography mass spectrometry (Sharp 1990) on a Thermo Mat 253 gas source mass spectrometer, following the methods described in Pack and Herwartz (2014). The $\Delta'^{17}O$ is defined as $\Delta'^{17}O = 1000*\ln(\delta^{17}O/1000 + 1) - 0.5305*1000*\ln(\delta^{18}O/1000 + 1)$. The oxygen isotope composition is normalized to the revised value of San Carlos olivine of $\Delta'^{17}O_{0.5305} = -51$ ppm (Pack et al. 2016). The $\delta^{17}O$ and $\delta^{18}O$ values are reported relative to VSMOW2.

Ca Isotopes

Powder aliquots of about 0.15 g were digested and processed for Ca isotope analysis by thermal ionization mass spectrometry (TIMS, Thermo Scientific Triton) at the Jet Propulsion Laboratory, Caltec following previously established methods (Dauphas et al. 2014). Calcium isotope anomalies are reported as parts per 10,000 deviation (ε-notation) from the terrestrial NIST SRM 915a standard after mass bias correction assuming the exponential law and $^{42}Ca/^{44}Ca = 0.31221$.

Ti Isotopes

Roughly half a gram of the sample powders and the BHVO-2 basalt standard were dissolved in 12 mL of a mixture of $HF:HNO_3:HClO_4$ at the Origins Lab, University of Chicago. The large sample sizes stem from the fact that not only Ti but also Mo and W isotope compositions were obtained from the same digested sample solutions. After removal of the main matrix elements by cation exchange column chromatography (15 mL AG50W-X8, 200–400 mesh) in HCl-HF media, Ti(+Zr,Hf), W, and Mo cuts were separated on an anion exchange column (4 mL AG1-X8, 200–400 mesh) broadly following previously established elution schemes (Kleine et al. 2004; Burkhardt et al. 2011). The Ti cut was then further purified on TODGA (2 mL) and AG1-X8 (0.8 mL, 200–400 mesh) chromatographic columns (Zhang et al. 2011). Titanium isotope measurements were made using the Origins Lab Thermo Scientific Neptune multicollector inductively coupled plasma–mass spectrometer (MC-ICP-MS) in high-resolution mode (Zhang et al. 2011). Solutions containing about 200 ppb Ti were introduced through a Cetac Aridus II desolvating system, resulting in a $\sim 4 \times 10^{-10}$ A ion beam on ^{48}Ti. Measurements consisted of a 30 s baseline measurement (deflected beam) followed by 20 isotope ratio measurements of 16 s each. Mass bias was corrected using the exponential law and $^{49}Ti/^{47}Ti = 0.749766$. Titanium isotope anomalies are reported as parts per 10,000 deviation (ε-notation) from the terrestrial OL-Ti (Millet and Dauphas 2014) bracketing standard.

Cr Isotopes

Between 0.005 and 0.04 g aliquots of the Allende, NWA 5363/NWA 5400, and BHVO-2 powders were digested and processed at USTC for Cr isotope analysis by Thermo Scientific Triton Plus TIMS at the State Key Laboratory of Geological Processes and Mineral Resources, University of Geosciences, Beijing, China following the protocol described in Qin et al. (2010), except that only conventional acid digestion of the samples with HNO_3 and HF was used. Results are presented in ε-units relative to the NIST SRM 3112a Cr standard after mass bias correction assuming the exponential law and a constant $^{50}Cr/^{52}Cr$ of 0.051859.

Ni Isotopes

Between 0.04 and 0.07 g of the sample powder was digested in $HF:HNO_3$ and aqua regia and Ni was separated using chromatography columns filled with

cation (5 mL AG50-X12, 200–400 mesh) and anion (1 mL Bio-Rad AG1W-X8, 200–400 mesh) resin at the Origins Lab following the protocol described by Tang and Dauphas (2012). Nickel isotope compositions were measured in medium resolution using the Origins Lab MC-ICP-MS equipped with a Cetac Aridus II introduction system. The samples were introduced into the mass spectrometer with Ar + N_2 and the instrument sensitivity for ^{58}Ni was ~10^{-9} A/ppm. One analysis was composed of 25 isotope ratio measurements of 8.4 s each. In one session, each sample solution was measured 13–15 times bracketed by SRM 986. Isobaric interference from ^{58}Fe (on ^{58}Ni) and ^{64}Zn (on ^{64}Ni) was monitored through ^{57}Fe and ^{66}Zn, respectively. The results are given in ε-units relative to the NIST SRM 986 Ni standard after mass bias correction assuming the exponential law and a constant ^{61}Ni/^{58}Ni ratio of 0.016730.

Mo Isotopes

The Mo cuts obtained from the Ti chemistry were further purified by two passes on TRU spec cation exchange resin in HNO_3 and HCl media (Burkhardt et al. 2011, 2014). The Mo isotopic composition was measured using the Origins Lab Neptune MC-ICP-MS in low-resolution mode. A Cetac Aridus II introduction system and normal H cones resulted in ion beam intensities of ~2.2×10^{-11} A on ^{96}Mo for 50 ppb measurement solutions. Measurements consisted of 30 s baseline integration (deflected beam) followed by 60 isotope ratio measurements of 4.2 s each. Mass bias was corrected by fixing the ^{98}Mo/^{96}Mo ratio to 1.453171 and using the exponential law. Blank (~1.3 ng Mo) and Zr and Ru interference corrections were negligible or small compared to the measurement uncertainties. The Mo data are presented in ε-notation relative to the bracketing terrestrial in-house Alfa Aesar Mo standard.

Ru Isotopes

Ruthenium isotope compositions were obtained from 0.3 to 0.4 g powder aliquots. The sample powder was digested in Carius tubes with reverse aqua regia. Ruthenium was separated by cation exchange column chromatography (10 mL AG50W-X8, 100–200 mesh) and further purified by microdistillation of Ru as RuO_4 into HBr from a H_2SO_4-CrO_3 solution (Fischer-Gödde et al. 2015). Measurements were performed using the NeptunePlus MC-ICP-MS at the University of Münster equipped with an Aridus II desolvator and conventional H cones, resulting in a total ion beam intensity of about 3×10^{-10} A for ~100 ppb Ru measurement solutions. Isotope analyses consisted of 40 × 8.4 s on-peak baseline integrations on a solution blank followed by 100 integrations of 8.4 s each on the sample or standard solutions. Mass bias was corrected using the exponential law and ^{99}Ru/^{101}Ru = 0.7450754. Ruthenium data are reported in ε-notation relative to bracketing Ru in-house solution standard (Alfa Aesar Ru).

W Isotopes

The W cuts obtained from the Ti chemistry were purified by an additional pass over an anion exchange column (1 mL AG1x8, 200–400 mesh) in HCl-HF-H_2O_2 media (Kleine et al. 2012). The W isotope compositions were measured using the Origins Lab Neptune MC-ICP-MS in low-resolution mode equipped with an Aridus II introduction system and a X skimmer cone and Jet-sampler cone setup. This setup resulted in ion beam intensities of 4×10^{-11} A on ^{183}W for 30 ppb measurement solutions. Measurements consisted of 30 s baseline integration (deflected beam), followed by 60 integrations of 4.2 s each. Mass bias was corrected by fixing the ^{186}W/^{184}W ratio to 0.92767 and using the exponential law. Blank (1.1 ng) and interference corrections were negligible or small compared to the measurement uncertainties. Tungsten data are reported relative to the bracketing in-house W standard (Spex CertiPrep) in ε-notation. Hafnium and W concentration data of NWA 5363/NWA 5400 were obtained from spiked aliquots of the digestion at the Institut für Planetologie, Münster.

RESULTS

Petrography

Figure 1 shows SEM backscattered electron images of NWA 5363 and NWA 5400. The texture of NWA 5363 and NWA 5400 is granoblastic with triple junctions and grain sizes mainly between 200 and 800 μm. Both meteorites show significant terrestrial alteration (Fe-oxide veins), with NWA 5363 being better preserved than NWA 5400. Consistent with previous petrographic investigations (Irving et al. 2009; Day et al. 2012; Gardner-Vandy et al. 2013; Weisberg et al. 2009–for NWA 5400; Garvie 2012; Larouci et al. 2013–for NWA 5363), olivine (Fa_{30}) is dominant (~80%) in both meteorites, followed by Ca-rich pyroxene ($En_{45}Fs_{10}Wo_{45}$), Ca-poor pyroxene ($En_{73}Fs_{25}Wo_2$), and minor chromite (Cr/Cr+Al=82), chlorapatite, troilite, (oxidized) Fe-Ni-metal grains ($Fe_{84.2}Ni_{14.7}Co_{1.1}$), and traces of plagioclase ($Ab_{72}An_{27}Or_1$). Troilite is found in association with metals, in ubiquitous veins along grain boundaries and as tiny inclusions in olivine and pyroxene. Taken together, the observed identical mineralogy and texture support a proposed paired origin of the two meteorites (Garvie 2012).

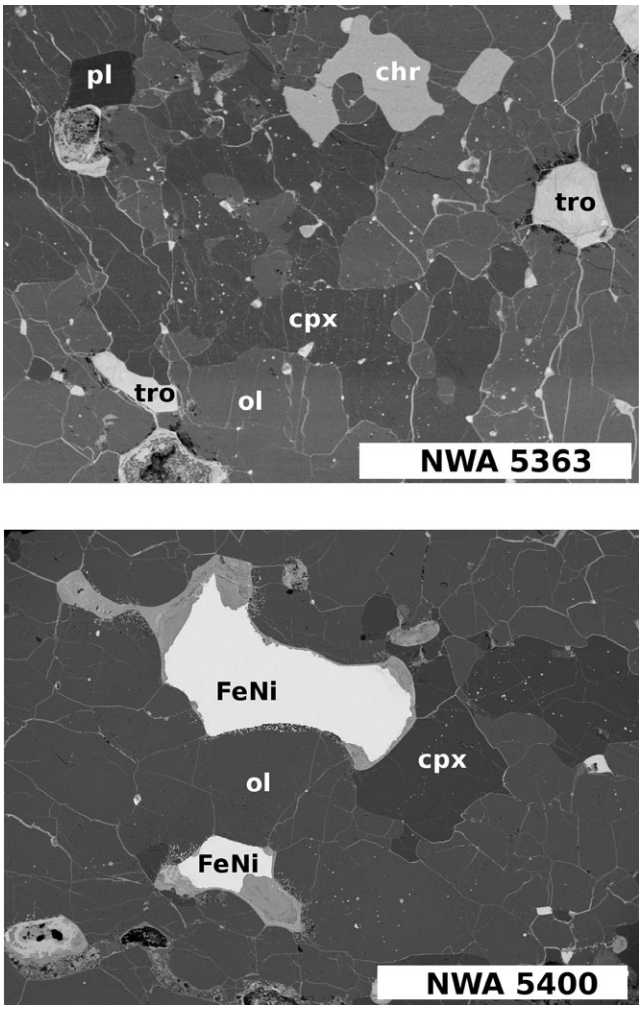

Fig. 1. SEM backscattered electron images of representative areas of polished sections of NWA 5363 and NWA 5400. The white scale bar is 1 mm long.

Major and Trace Elements

The bulk chemical compositions of the NWA 5363/NWA 5400/NWA 5400alt samples and the Allende Smithsonian reference powder are given in Table 1. The compositional data obtained for Allende are within error limits identical to the reference values (Jarosewich et al. 1987), for both major and trace elements. The notable exception is W for which an about 7× higher concentration was obtained here (1.12 ppm versus 0.16 ppm), most likely the result of impurities in the fluxing agent used by the SARM, Nancy. As the W (and Hf) concentrations of NWA 5363 and NWA 5400 were also determined by isotope dilution in Münster, this inaccuracy is of no significance, however. We also note that the Mo content of the Allende Smithsonian reference powder is a factor of ~2 higher than that determined for other Allende samples (e.g., Burkhardt et al. 2011; Stracke et al. 2012), possibly reflecting Mo contamination during the production of the reference powder. In any case, the good agreement between Jarosewich et al. (1987) and our data (except for W) highlights the accuracy of the SARM analyses.

The elemental compositions of NWA 5363, NWA 5400, and NWA 5400alt are very similar to each other for most analyzed elements, providing further evidence for the paired nature of the NWA 5363 and NWA 5400 meteorites. The largest variability between the three analyzed NWA samples is seen for elements tracing desert weathering, like Sr, Ba, and U, with NWA 5400alt showing the highest concentrations (e.g., 195 ppm Ba) followed by NWA 5400 (80.5 ppm) and NWA 5363 (<1.6 ppm). This grading is consistent with visual examination of the rock slices and the sample powders, and confirms that our NWA 5363 sample is least affected by terrestrial weathering. Relative to chondritic abundances, the NWA samples are depleted in incompatible lithophile Al, Na, K, Ti, HFSEs, and REEs (Fig. 2), consistent with a restite-like mineralogy. Molybdenum and W (and the HSE; Day et al. 2012) on the other hand show enrichments relative to chondrites (Mo~2 × CI, W~10 × CI, Ir,Os~5 × CI).

Isotope Compositions

The isotope compositions of the measured chondrites, NWA 5363/NWA 5400 samples, and terrestrial standards are given in Table 2 and are shown in Figs. 3–5 for the isotope notation most frequently used to express isotope anomalies (i.e., $\Delta^{17}O$, $\varepsilon^{48}Ca$, $\varepsilon^{50}Ti$, $\varepsilon^{54}Cr$, $\varepsilon^{62}Ni$, $\varepsilon^{92}Mo$, $\varepsilon^{100}Ru$, and $\varepsilon^{182}W$). The full isotope data are available in Table S1 in the supporting information.

Oxygen

The $\delta^{18}O$ and $\Delta^{17}O$ values of NWA 5363 ($+5.7 \pm 0.7$; -0.045 ± 0.020; 2σ) and NWA 5400 ($+6.7 \pm 0.7$; -0.088 ± 0.032) are within uncertainty indistinguishable from the BHVO-2 ($+5.7 \pm 0.7$; -0.037 ± 0.032) and San Carlos olivine ($+5.3 \pm 0.7$; -0.051 ± 0.012) standard measurements. These results confirm earlier O isotope measurements that found no $\Delta^{17}O$ anomalies in the NWA 5363/NWA 5400 samples relative to the Earth (Irving et al. 2009; Shukolyukov et al. 2010; Larouci et al. 2013). At the 1σ level, the $\Delta^{17}O$ values of NWA 5363 and NWA 5400 are distinct. This most likely reflects the effects of desert alteration on NWA 5400. Oxygen isotope data for Allende and Allegan are within the range of literature data for CV and H chondrites. Our measurement of Pillistfer confirms a significant (~50 ppm) difference in $\Delta^{17}O$ between enstatite chondrites and the Earth (Herwartz

Table 1. Major and trace element composition of the Allende Smithsonian reference powder and NWA 5363, NWA 5400, and NWA 5400alt samples

wt%	Allende	NWA 5363	NWA 5400	NWA 5400 altered
SiO_2	34.80 ± 0.70	34.87 ± 0.70	36.68 ± 0.73	34.97 ± 0.70
Al_2O_3	3.39 ± 0.07	0.30 ± 0.07	0.19 ± 0.05	0.19 ± 0.05
Fe_2O_3 (Fe tot.)	33.99 ± 0.68	32.83 ± 0.66	30.83 ± 0.62	31.87 ± 0.64
MnO	0.22 ± 0.02	0.38 ± 0.04	0.42 ± 0.04	0.39 ± 0.04
MgO	25.0 ± 0.5	28.89 ± 0.58	30.03 ± 0.60	28.25 ± 0.56
CaO	2.64 ± 0.16	1.54 ± 0.09	1.96 ± 0.12	2.40 ± 0.14
Na_2O	0.46 ± 0.09	0.08 ± 0.02	0.05 ± 0.01	0.05 ± 0.02
K_2O	0.05 ± 0.01	0.01 ± 0.01	<0.01	0.02 ± 0.01
TiO_2	0.15 ± 0.03	0.03 ± 0.01	0.04 ± 0.02	0.03 ± 0.02
P_2O_5	0.25 ± 0.05	0.30 ± 0.06	0.22 ± 0.04	0.25 ± 0.05
FeO		24.57 ± 0.05	22.65 ± 0.05	22.14 ± 0.05
S total	1.96 ± 0.01	1.71 ± 0.01	0.35 ± 0.01	0.90 ± 0.01
CO_2 total	0.74 ± 0.01	<0.01	0.42 ± 0.01	0.42 ± 0.01
LOI	−2.09	−0.40	−0.41	0.10
Total	98.88	98.82	100.01	98.53
ppm				
Sc	11.50 ± 3.45	7.82 ± 3.91	9.54 ± 2.86	10.75 ± 3.23
V	89.7 ± 9.0	71.52 ± 7.15	103.9 ± 10.4	84.84 ± 8.48
Cr	3558 ± 213	3770 ± 226	5750 ± 345	3475 ± 209
Co	604 ± 36	475 ± 28.52	269 ± 16	458 ± 27
Ni	14210 ± 1421	6756 ± 676	3219 ± 322	4573 ± 457
Cu	89.8 ± 9.0	28.46 ± 5.69	9.31 ± 1.86	20.48 ± 4.10
Zn	120 ± 24	77 ± 15	78 ± 16	59 ± 12
Ga	6.05 ± 0.97	1.78 ± 0.28	2.327 ± 0.37	1.92 ± 0.31
Ge	15.9 ± 1.6	38.52 ± 3.85	23.43 ± 2.34	58.9 ± 3.53
As	2.34 ± 1.17	2.36 ± 1.18	<1.5 ±	2.68 ± 0.00
Rb	1.23 ± 0.25	0.69 ± 0.34	<0.4 ±	0.58 ± 0.29
Sr	13.67 ± 2.73	2.62 ± 1.31	13.01 ± 2.60	20.02 ± 4.00
Y	2.51 ± 1.25	0.79 ± 0.40	0.58 ± 0.29	1.03 ± 0.52
Zr	6.82 ± 3.41	1.08 ± 0.54	1.35 ± 0.67	3.32 ± 1.66
Nb	0.49 ± 0.15	0.15 ± 0.03	<0.09	<0.09
Mo	2.76 ± 0.55	2.63 ± 0.53	0.67 ± 0.33	1.35 ± 0.27
Cd	0.60 ± 0.30	<0.12	<0.12	<0.12
In	0.13 ± 0.07	0.15 ± 0.08	<0.07	0.07 ± 0.04
Sn	0.86 ± 0.43	0.514 ± 0.26	<0.45	<0.45
Sb	<0.20	<0.20	<0.20	<0.20
Cs	0.11 ± 0.05	<0.1	<0.1	<0.1
Ba	3.26 ± 1.63	<1.6	80.49 ± 8.05	195 ± 20
La	0.48 ± 0.10	<0.09	<0.09	0.22 ± 0.04
Ce	1.19 ± 0.24	<0.14	<0.14	0.45 ± 0.22
Pr	0.191 ± 0.038	0.019 ± 0.004	0.021 ± 0.004	0.061 ± 0.012
Nd	0.888 ± 0.178	0.115 ± 0.023	0.115 ± 0.023	0.256 ± 0.051
Sm	0.289 ± 0.058	0.044 ± 0.022	0.063 ± 0.032	0.087 ± 0.044
Eu	0.096 ± 0.010	0.018 ± 0.004	0.016 ± 0.003	0.031 ± 0.006
Gd	0.337 ± 0.034	0.062 ± 0.012	0.082 ± 0.016	0.112 ± 0.011
Tb	0.055 ± 0.011	0.008 ± 0.002	0.015 ± 0.003	0.021 ± 0.004
Dy	0.394 ± 0.079	0.076 ± 0.023	0.091 ± 0.027	0.155 ± 0.031
Ho	0.080 ± 0.040	0.017 ± 0.009	0.026 ± 0.013	0.035 ± 0.018
Er	0.243 ± 0.049	0.055 ± 0.028	0.074 ± 0.037	0.106 ± 0.021
Tm	0.046 ± 0.023	0.008 ± 0.004	0.012 ± 0.006	0.015 ± 0.008
Yb	0.279 ± 0.056	0.069 ± 0.035	0.083 ± 0.042	0.123 ± 0.025
Lu	0.038 ± 0.008	0.013 ± 0.003	0.018 ± 0.004	0.019 ± 0.004
Hf	0.17 ± 0.05	0.0059 ± 0.0002	0.0093 ± 0.0002	0.06 ± 0.03

Table 1. *Continued*. Major and trace element composition of the Allende Smithsonian reference powder and NWA 5363, NWA 5400, and NWA 5400alt samples.

wt%	Allende	NWA 5363	NWA 5400	NWA 5400 altered
Ta	0.05 ± 0.03	0.19 ± 0.06	<0.01	<0.01
W[a]	1.12 ± 0.33	1.065 ± 0.015	0.930 ± 0.015	*2.13* ± 0.64
Pb	3.12 ± 0.62	1.99 ± 0.40	2.46 ± 0.49	2.89 ± 0.58
Bi	0.26 ± 0.13	<0.1	<0.1	<0.1
Th	<0.06	<0.06	<0.06	<0.06
U	0.07 ± 0.04	0.07 ± 0.04	0.13 ± 0.04	0.28 ± 0.08

[a]W concentration of Allende and NWA 5400 altered is compromised by impurities in the fluxing agent.

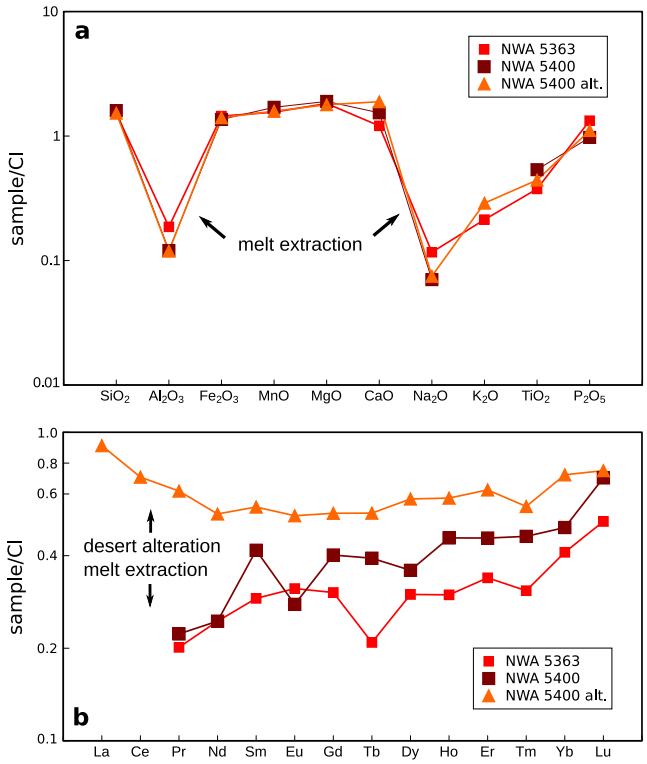

Fig. 2. Major element (a) and REE (b) composition of NWA 5363, NWA 5400, and NWA 5400alt relative to CI chondrites. Major element composition is relatively uniform and shows depletions in Al, Na, and Ti, consistent with the restite mineralogy and the removal of a silicate melt. REE patterns are also indicative of a melt depletion. Higher REE concentrations in NWA 5400alt, and (to a lesser degree) in NWA 5400, relative to NWA 5363 imply that the latter is least affected by desert alteration. (Color figure can be viewed at wileyonlinelibrary.com.)

et al. 2014), leaving NWA 5363/NWA 5400 as the only known meteorite with identical $\Delta^{17}O$ as the Earth.

Calcium

Our data show a common, and relative to the Earth, slightly anomalous Ca isotope composition of NWA 5363 and NWA 5400 ($\varepsilon^{48}Ca = -0.55 \pm 0.22$ and -0.48 ± 0.40, respectively) (Fig. 4). The anomalies are similar to the ones reported for ordinary and enstatite chondrites (Dauphas et al. 2014a).

Titanium

The Ti isotope compositions of NWA 5363 and NWA 5400 ($\varepsilon^{50}Ti = -1.00 \pm 0.14$ and -1.03 ± 0.11) are within uncertainty identical to each other, but significantly different from the terrestrial standard composition. Data for Allende, Allegan, and Pillistfer agree within error with literature values of the CV, H, and EL chondrite groups (Trinquier et al. 2009; Zhang et al. 2012).

Chromium

Similar to Ca and Ti, the Cr isotope compositions of NWA 5363 and NWA 5400 are identical and slightly depleted in the neutron-rich isotopes, resulting in a mean $\varepsilon^{54}Cr$ value of -0.37 ± 0.13. This value is different from the $\varepsilon^{54}Cr$ of 0.07 ± 0.11 reported by Shukolyukov et al. (2010) for NWA 5400 in a conference proceeding. As no information was provided on the analytical procedures used in the latter study, the reason for this discrepancy remains uncertain. We note that in a recent conference abstract, an $\varepsilon^{54}Cr$ value of -0.27 ± 0.08 was reported for NWA 5400 (Sanborn et al. 2016), in line with our data. We also note that the Cr isotope datum for Allende is consistent with our previous work (Qin et al. 2010).

Nickel

The Ni isotope compositions of NWA 5363 and NWA 5400 are indistinguishable from each other ($\varepsilon^{64}Ni = +0.05 \pm 0.19$ and $+0.03 \pm 0.08$) and within uncertainty of the terrestrial standard composition ($\varepsilon^{64}Ni = 0$). The Ni isotope data of the chondrites agree within error with literature values (Regelous et al. 2008; Steele et al. 2011; Tang and Dauphas 2012).

Molybdenum

NWA 5363 is characterized by a small deficit in *s*-process Mo ($\varepsilon^{92}Mo = 0.53 \pm 0.22$), similar to the values of Allegan, Pillistfer, and other ordinary and

Table 2. Oxygen, Ca, Ti, Cr, Ni, Mo, Ru, and W isotope composition of Allende (CV3), Allegan (H6), Pillistfer (EL6), NWA 5363, NWA 5400, and terrestrial rock standards.

Sample	$\Delta^{17}O_{SC}$[a] ± $2\sigma_{SE}$	$\varepsilon^{48}Ca$ ± 95% CI	$\varepsilon^{50}Ti$ ± 95% CI	$\varepsilon^{54}C$ ± 95% CI	$\varepsilon^{64}Ni$ ± 95% CI	$\varepsilon^{92}Mo$ ± 95% CI	$\varepsilon^{100}Ru$ ± $2\sigma_{SD}$	$\varepsilon^{182}W$ ± 95% CI
BHVO-2	0.01 ± 0.03	0.00[b] ± 0.14	−0.15 ± 0.13	−0.01 ± 0.13	0.09[c] ± 0.12	0.07 ± 0.30	0.07[d] ± 0.03	0.33 ± 0.20
Pillistfer EL6	0.05 ± 0.03		−0.15 ± 0.27		−0.08 ± 0.12	0.67 ± 0.30		−2.01 ± 0.37
Allegan H5	0.71 ± 0.03		−0.61 ± 0.29		−0.06 ± 0.09	0.84 ± 0.34	−0.33 ± 0.13	−1.84 ± 0.12
Allende CV3	−3.66 ± 0.03		3.48 ± 0.17	0.90 ± 0.12	0.34 ± 0.06	2.00 ± 0.16	−1.01 ± 0.05	−1.78 ± 0.17
NWA 5363	0.01 ± 0.02	−0.55 ± 0.22	−1.00 ± 0.14	−0.31 ± 0.24	0.05 ± 0.19	0.53 ± 0.22	−0.34 ± 0.13	−3.26 ± 0.08
NWA 5400	−0.04 ± 0.03	−0.48 ± 0.40	−1.03 ± 0.11	−0.40 ± 0.15	0.03 ± 0.08			−3.18 ± 0.08
wt. av. NWA 5363/NWA 5400	−0.01 ± 0.02	−0.53 ± 0.20	−1.02 ± 0.09	−0.37 ± 0.13	0.04 ± 0.08	0.53 ± 0.22	−0.34 ± 0.13	−3.22 ± 0.06

[a]$\Delta^{17}O$ are given relative to the values measured for San Carlos Olivine.
[b]BHVO-2 data from Dauphas et al. (2014a).
[c]Ni data for DTS-2 standard.
[d]BHVO-2 and Allende data from Fischer-Gödde et al. (2015). Due to the low Ru abundance, BHVO-2 was doped with Ru standard to illustrate the absence of matrix effects.

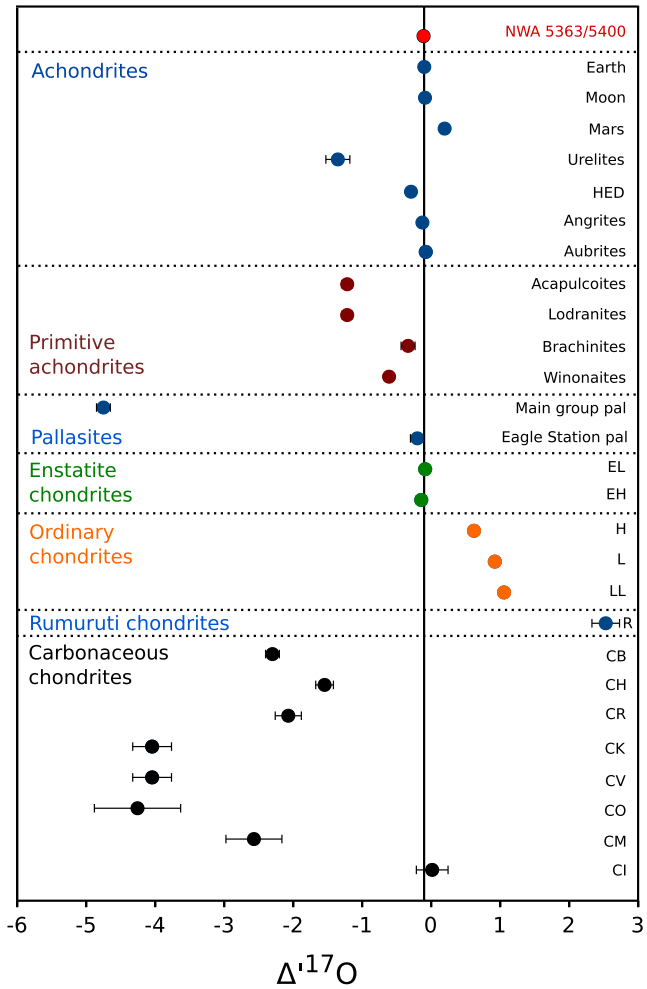

Fig. 3. $\Delta^{17}O$ of NWA 5363/NWA 5400 in comparison with chondrites, pallasites, and achondrites. Bulk Earth (as represented by San Carlos olivine at −0.05‰ relative to VSMOW=0; Pack et al. 2016) is identical to the $\Delta^{17}O$ of NWA 5363/NWA 5400. (Color figure can be viewed at wileyonlinelibrary.com.)

enstatite chondrites (Fig. 5). The datum obtained here for Allende ($\varepsilon^{92}Mo = +2.00 \pm 0.16$) is significantly lower than the one obtained by Burkhardt et al. (2011) ($\varepsilon^{92}Mo = 3.35 \pm 0.36$) on another Allende powder. The explanation for this discrepancy is most likely heterogeneity at the sampling scale, e.g., the amount of CAI material in different Allende powders (Budde et al. 2016).

Ruthenium

Similar to Mo, the Ru isotope composition of NWA 5363 exhibits a *s*-process deficit ($\varepsilon^{100}Ru = -0.34 \pm 0.13$) akin to that found in Allegan and other ordinary chondrites (Fischer-Gödde et al. 2015).

Tungsten

No nucleosynthetic W isotope anomalies are resolvable for any of the samples ($\varepsilon^{184}W = \varepsilon^{183}W = 0$) (see Data S1 ub supporting information). Thus, the measured $\varepsilon^{182}W$ values of the samples can be directly interpreted in terms of decay of the short-lived ^{182}Hf-^{182}W system, a prime chronometer for establishing the time scale of planetary differentiation in the early solar system (Kleine et al. 2009). NWA 5363 and NWA 5400 exhibit identical and highly unradiogenic $\varepsilon^{182}W$ values of -3.26 ± 0.08 and -3.18 ± 0.08, as well as very low $^{180}Hf/^{184}W$ ratios of 0.0065 ± 0.0002 and 0.0118 ± 0.0003, respectively.

DISCUSSION

Our new petrographic, elemental, and isotopic data provide strong evidence that NWA 5363 and NWA 5400 are paired primitive achondritic meteorites from an asteroidal parent-body not previously sampled in our collections. In the following, we use the available petrological and chronological information to constrain the formation and differentiation history of the NWA 5363/NWA 5400 parent-body and then discuss its isotopic composition with respect to other planetary bodies, mixing in the protosolar nebula, and the composition of the Earth.

Formation and Differentiation History of the NWA 5363/NWA 5400 Parent-Body

Petrological Constraints

The closest meteoritic analog to the NWA 5363/NWA 5400 meteorite samples are brachinites, a group of primitive achondrites with which they share most petrologic characteristics, i.e., equilibrated textures, FeO-rich silicates ($Fa_{\sim 30}$), and an olivine-dominated depleted mineralogy, but whose O isotopic composition is markedly different (Irving et al. 2009; Day et al. 2012; Gardner-Vandy et al. 2013). Primitive achondrites are interpreted to be relics from asteroidal bodies of chondritic composition whose internal heating was sufficient to induce partial melting, but not strong enough to cause global melting and complete differentiation into core, mantle, and crust. Thus, primitive achondrites form an intermediary between the undifferentiated chondrites and the samples from fully differentiated bodies like Mars, Vesta, the Moon or the parent bodies of angrites and the magmatic iron meteorites. These features make them valuable samples for studying the initial stages of planetary differentiation. Brachinites and the brachinite-like achondrite NWA 5400 have been recently studied in detail by several groups. Although it was previously argued that brachinites may have a cumulate origin

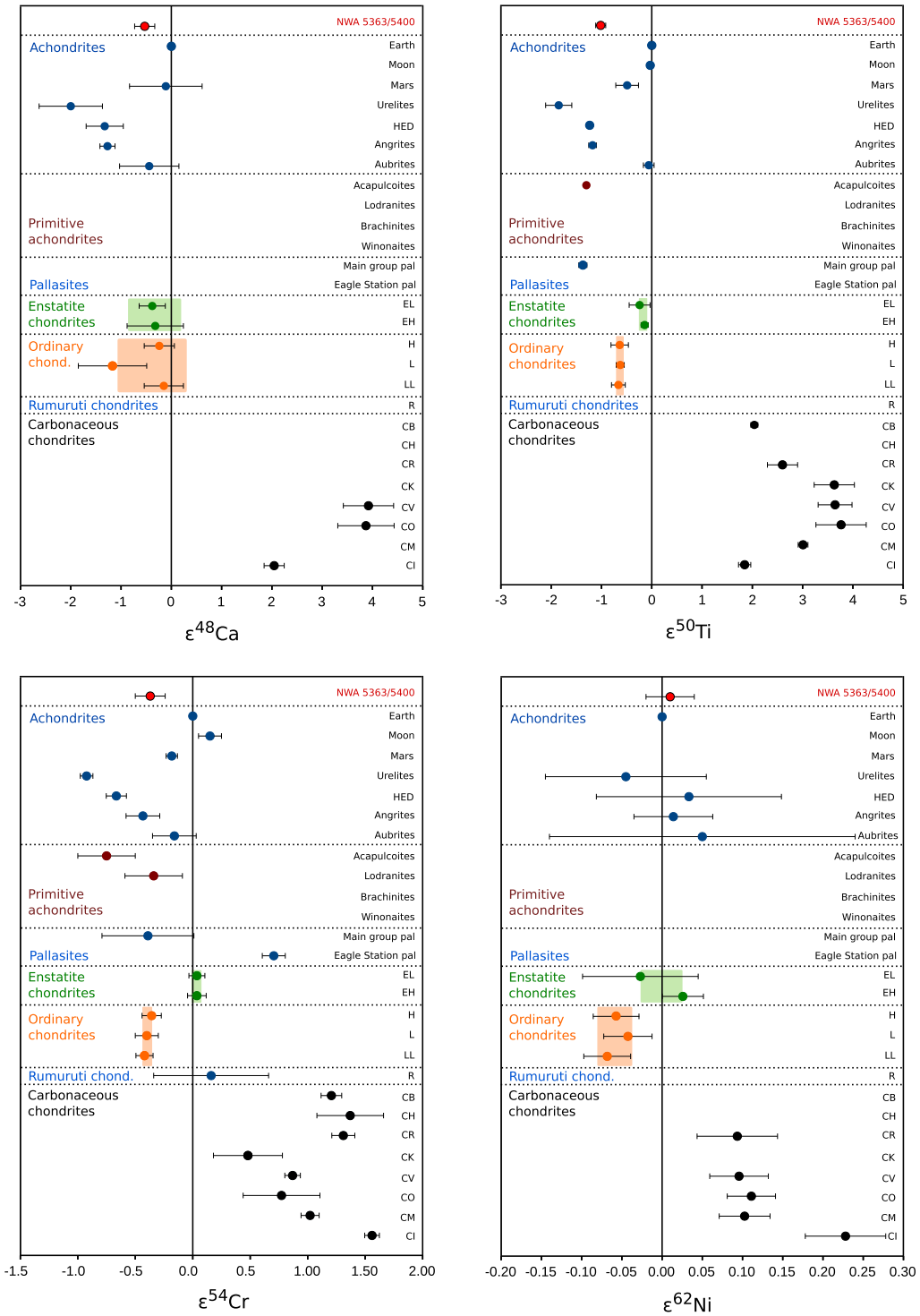

Fig. 4. Nucleosynthetic variations of NWA 5363/NWA 5400 and planetary materials for Fe-group elements Ca, Ti, Cr, and Ni. For all elements but Ni, the isotopic composition of NWA 5363/NWA 5400 is significantly different from the composition of the Earth. Mean values of ordinary and enstatite chondrite groups are represented by their 95% confidence intervals as shaded areas. Data sources: this study and Ca: Chen et al. (2011); Dauphas et al. (2014a); Ti: Trinquier et al. (2009); Zhang et al. (2012); Cr: Shukolyukov and Lugmair (2006); Trinquier et al. (2007); Shukolyukov et al. (2009); Qin et al. (2010); Göpel and Birck (2010); Yamakawa et al. (2010); Larsen et al. (2011); Schiller et al. (2014); Göpel et al. (2015); Ni: Regelous et al. (2008); Steele et al. (2011); Tang and Dauphas (2012, 2014). (Color figure can be viewed at wileyonlinelibrary.com.)

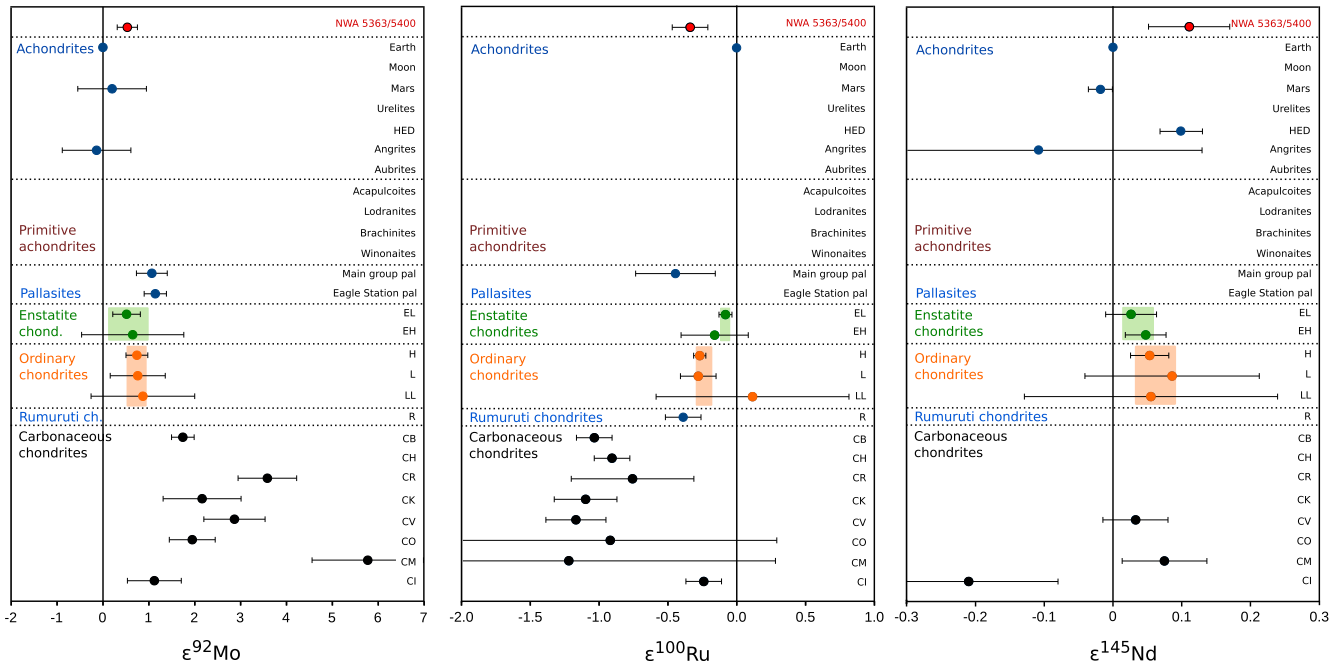

Fig. 5. Mo, Ru, and Nd isotope compositions of NWA 5363/NWA 5400 and other planetary bodies. Please note that the anomalies in these elements are correlated with each other, reflecting variable *s*-process deficits relative to the terrestrial isotope composition. The exceptions are the Nd anomalies in carbonaceous chondrites, which are biased toward the negative ε^{145}Nd anomalies of CAIs (Burkhardt et al. 2016). Mean values of ordinary and enstatite chondrite groups are represented by their 95% confidence intervals as shaded areas. Data sources: this study and Mo: Burkhardt et al. (2011, 2014); Dauphas et al. (2002); Ru: Chen et al. (2010); Fischer-Gödde et al. (2015); Fischer-Gödde and Kleine (2017); Nd: Borg et al. (2016); Boyet and Carlson (2005); Carlson et al. (2007); Sanborn et al. (2015); Andreasen and Sharma (2007); Gannoun et al. (2011); Burkhardt et al. (2016). (Color figure can be viewed at wileyonlinelibrary.com.)

(Warren and Kallemeyn 1989), the currently prevailing interpretation is that they formed by the extraction of a silica-saturated partial melt (~10–30%) from a chondritic source rock (Day et al. 2012; Gardner-Vandy et al. 2013; Usui et al. 2015). The silicate melt may be sampled by the oligoclase-rich evolved achondritic meteorites Graves Nunataks 06128/06129 (Day et al. 2009, 2012), while the brachinites represent the depleted ultramafic restite. With the removal of the silicate melt, further differentiation of the brachinite source region likely came to a halt, possibly because the melt deprived it from heat-producing elements, in particular incompatible ^{26}Al. The high total Fe and HSE concentration in the brachinites (and NWA 5400) seems to indicate that no large-scale metal-silicate differentiation occurred in the brachinite parent-body.

To obtain information on the brachinite precursor and the oxygen fugacity under which the brachinites formed, Gardner-Vandy et al. (2013) calculated equilibrium fO_2 and equilibrium temperatures of brachinites and NWA 5400 using the quartz-iron-fayalite system (QIFa), and the olivine-chromite thermometer (Sack and Ghiorso 1991) as well as the quartz-iron-ferrosilite system (QIFs) and the two-pyroxene thermometer. For NWA 5400, they obtained 1028 ± 22 °C and IW-1.1, and 909 ± 26 °C and IW-1.4, respectively. Combining the NWA 5363 and NWA 5400 mineral data from our study with all available literature data (Irving et al. 2009; Gardner-Vandy et al. 2013; Larouci et al. 2013), we have repeated the exercise for the two-pyroxene and Ca-in-opx thermometers (Brey and Köhler 1990) as well as the Ca-in-ol thermometer (Köhler and Brey 1990) and got equilibration temperatures of 959–1031 °C, 851–883 °C, and 897–1096 °C, respectively, with the range reflecting the 2σ uncertainties of the mean mineral compositions. Assuming equilibrium between opx and ol, we calculated the fO_2 according to

$$Fe_2SiO_4 = FeSiO_3 + Fe + 1/2O_2$$

with

$$K = \frac{a_{Fe}^{opx} \cdot a_{Fe}^{metal} \cdot (fO_2)^{1/2}}{a_{Fe}^{ol}} \approx \frac{X_{Fe}^{opx} \cdot X_{Fe}^{metal} (fO_2)^{1/2}}{(X_{Fe}^{ol})^2}$$

where K, a, and X refer to the equilibrium constant of the reaction, the activity of Fe, and the molar fraction of Fe in a mineral phase. Using the $Fa_{30.1}$ and $Fs_{25.4}$ mole fractions from the combined NWA 5363/NWA 5400 mineral data, a X_{Fe} of the NWA 5400 metal of

0.842 and the thermodynamic data set of Robie and Hemingway (1995) for calculating log*K*s, an oxygen fugacity of IW-1.21 is obtained for an equilibration temperature of 1000 °C. This implies that metal phases were stable and present during the melt extraction, such that siderophile elements were retained in the source, qualitatively consistent with the high Mo, W, and HSE concentrations measured in NWA 5363/NWA 5400. The bulk total Fe measured in the NWA 5363/NWA 5400 samples is ~22 ± 1 wt%, within the range of total Fe of bulk chondrites (19–28 wt%; Jarosewich 1990). Given the high FeO content of the silicates ($Fa_{30.1}$, $Fs_{25.4}$) and assuming a single-stage evolution without refertilization, this indicates that no more than ~5% of the total Fe has been lost by melt extraction from a chondritic source. As some Fe entered the silicate melt as Fe^{2+}, a significant Fe loss through large-scale metal-silicate fractionation, i.e., core formation on the NWA 5363/NWA 5400 parent-body seems unlikely. However, in order to explain the nonchondritic HSE signatures of NWA 5400, the extraction of a small amount of a high-S metallic melt from the chondritic source seems to be required (Day et al. 2012). As the Fe-Ni-S eutectic is below the silicate melting temperature, the removal of such a high-S melt may have occurred before or along with the silicate melt extraction. Furthermore, some of the siderophile elements, such as W, occur not only in nonchondritic proportions but are also highly enriched relative to a chondritic source rock. This can neither be solely caused by the loss of a small amount of a high-S melt nor by the extraction of 10–30% of a silica-saturated melt from a chondritic source, but requires a process that adds these elements. This might have happened by fluxing of silicate melt from a more oxidized source (where W is incompatible) through the NWA 5363/NWA 5400 source region (where W is scavenged), or by some high-S melts that were added either before or after the silicate melt extraction and produced the observed 5–10 × CI enrichments in W and some HSEs.

Chronological Constraints

Thus far, age constraints on the formation and evolution of the NWA 5363/NWA 5400 parent-body are sparse. Dating of NWA 5400 by U-Pb systematics did not yield an isochron of chronological significance, but only a mixing line between primordial Pb and modern terrestrial crustal Pb, which was introduced through terrestrial alteration. Based on the finding of primordial Pb, it was concluded that NWA 5400 derives from a parent-body that either differentiated early or did not lose its volatile elements (Amelin and Irving 2011). Samarium-Nd systematics suggest that the superchondritic Sm/Nd of NWA 5363 was acquired during an early silicate melt extraction event, as whole rock data fall within uncertainty on a 4.568 Ga chondrite isochron (Burkhardt et al. 2016). Assuming a chondritic initial $^{143}Nd/^{144}Nd$ yields a model age of 4547 ± 53 Ma for the long-lived ^{147}Sm-^{143}Nd system, and assuming an ordinary chondrite-like precursor (i.e., $\varepsilon^{142}Nd = -0.167$) forming at 4566 Ma yields an model age of 4566 ± 14 Ma for the short-lived ^{146}Sm-^{142}Nd system. For the ^{53}Mn-^{53}Cr system, an upper age limit of 4552 Ma before present was proposed for NWA 5400, because no evidence of live ^{53}Mn at the time of mineral closure was detected (Shukolyukov et al. 2010; Sanborn et al. 2016). This young apparent age contrasts with old ^{53}Mn-^{53}Cr crystallization ages (4564.5 ± 0.9) obtained for brachinites (Wadhwa et al. 1998) and either reflects protracted magmatic processes on the NWA 5400 parent-body or resetting of the chronometer during late-stage thermal events. Finally, an I-Xe age of 4568.9 ± 0.6 for closure in olivine and apatite was reported (Pravdivtseva et al. 2015), in apparent conflict with the young Mn-Cr age. In contrast to the U-Pb, Mn-Cr, and I-Xe systems, the Hf-W chronometer has the advantage of being less susceptible to postcrystallization disturbances like parent-body metamorphism or impact events and terrestrial alteration. Within uncertainty, our NWA 5363 and NWA 5400 samples exhibit identical and highly unradiogenic $\varepsilon^{182}W$ values of −3.26 ± 0.08 and −3.18 ± 0.08, as well as very low $^{180}Hf/^{184}W$ ratios of 0.0065 ± 0.0002 and 0.0118 ± 0.0003, respectively. Correcting for ^{182}Hf ingrowth yields initial $\varepsilon^{182}W$ values at the time of Hf-W fractionation of −3.27 ± 0.08 and −3.20 ± 0.08, the weighted average of which is −3.24 ± 0.06. Under the assumption that the NWA 5363/NWA 5400 parent-body evolved with a chondritic Hf/W ratio, a two-stage model age of the fractionation from a chondritic reservoir can be calculated using:

$$\Delta t_{\mathrm{CAI}} = -\frac{1}{\lambda} \times \ln\left[\frac{\in W_{\mathrm{sample}} - \in \mathrm{W_{CHUR}}}{\in \mathrm{W_{SSI}} - \in \mathrm{W_{CHUR}}}\right]$$

where Δt_{CAI} is the time after formation of the solar system in million years, $\lambda = 0.0778 \pm 0.0015\ \mathrm{Ma}^{-1}$ is the ^{182}Hf decay constant (Vockenhuber et al. 2004), $\varepsilon^{182}W_{\mathrm{sample}}$ is the initial W isotopic composition of NWA 5363/NWA 5400, $\varepsilon^{182}W_{\mathrm{CHUR}} = -1.9 \pm 0.1$ is the present-day W isotopic composition of chondrites (Kleine et al. 2009), and $\varepsilon^{182}W_{\mathrm{SSI}} = -3.49 \pm 0.07$ is the solar system initial W isotopic composition as inferred from CAI (Kruijer et al. 2014). For the mean $\varepsilon^{182}W_i$ of −3.24 ± 0.06 of the NWA samples, this equates to a two-stage model age of Hf/W fractionation from a chondritic reservoir of 2.2 ± 0.8 Myr after CAI formation.

This age is similar to the I-Xe age, but what is its significance and which event(s) does it date? As

discussed in the previous section, at least two processes are needed to explain the element concentration patterns of NWA 5363/NWA 5400—the extraction of a silicate melt at a time $t_{sil.\ ext.}$ and the addition of W (and some other siderophile elements) at a time $t_{W\ add.}$ after the start of the solar system. Both processes decreased the Hf/W ratio of the reservoir, the former by removal of Hf, the latter by addition of W. The W addition either happened before ($t_{W\ add.} < t_{sil.\ ext.}$), after ($t_{W\ add.} > t_{sil.\ ext.}$), or at the same time ($t_{W\ add.} = t_{sil.\ ext.}$) as the silicate melt extraction.

In the latter case ($t_{W\ add.} = t_{sil.\ ext.}$), the calculated model age of 2.2 Ma after CAI actually dates this event. In the case where the W addition happened before the melt extraction ($t_{W\ add.} < t_{sil.\ ext.}$), the model age can be interpreted as the latest possible time after CAI formation at which the W addition could have taken place. The timing of silicate melt extraction is dependent on the time of W addition in this scenario. If the W addition was earlier than 2.2 Ma, then the melt extraction must have happened after this date. The minimum age of W addition is ~0.8 Ma after CAI, because a reservoir with ~10 × CI W separating from the chondritic evolution at that time would evolve to an $\varepsilon^{182}W = -3.24$ even without extracting a Hf-rich silicate melt at a later time. Thus, in case of an early W addition, the timing of silicate melt extraction could be significantly underestimated by the 2.2 Ma model age and in fact this event may only have happened after the extinction of the ^{182}Hf-^{182}W system (>50 Ma after CAI). In the last possible scenario, silicate melt extraction precedes W addition ($t_{W\ add.} > t_{sil.\ ext.}$) and thus the 2.2 Ma model age represents a maximum age of melt extraction and a minimum age of W addition. A maximum age of W influx of ~2.4 Ma after CAI can be equated by adding W from a chondritic reservoir to a melt-depleted ($^{180}Hf/^{184}W$ ~0.1) and early-formed (t = 0 Ma) reservoir in a ratio of 9:1, such that today's amounts of Hf and W and a $\varepsilon^{182}W$ of −3.24 are obtained.

Taken together, most of the scenarios discussed above imply a relatively close temporal relation between the W addition and the silicate melt extraction, such that the calculated model age of 2.2 ± 0.8 Ma after CAI most likely dates both of these events within the error limits. Although possible, the scenario where an early W addition by percolating low-degree Fe-S melts is followed by melt extraction millions of years later is not supported by the I-Xe age and the petrographic observations. The SEM pictures show ubiquitous Fe-S veins forming networks along grain boundaries, indicating low-degree Fe-S melts percolating through the rocks after the silicate extraction. Thus, the W addition probably succeeded the silicate melt extraction and both events happened within 3 Ma after CAI formation.

Synthesis

Based on the peridotitic mineralogy and the terrestrial O isotopic composition, it was speculated that NWA 5363 and NWA 5400 might be terrene meteorites detached from the Earth early in its history, remnants of the putative Moon-forming impact, or samples from a former differentiated planetary body that accreted close to the Earth (Irving et al. 2009; Larouci et al. 2013; Dauphas et al. 2014a, 2014b). While these speculations are certainly thought-provoking and sparked our initial interest in these rocks, the petrographic, chronological, and isotopic (see discussion below) results obtained here do not support such a relationship. Incompletely differentiated rocks with a formation age of <3 Ma after CAI are unlikely to survive on large planetary bodies like the proto-Earth or the Moon-forming impactor because the accretion and differentiation history of these bodies would have erased any such early signatures. Furthermore, preserving meteorites ejected from the early Earth, e.g., during the late heavy bombardment or during the Moon-forming impact for billions of years seems also highly unlikely from a dynamical perspective (e.g., Bottke et al. 2006). Instead our results imply the origin of NWA 5363/NWA 5400 from a partially differentiated asteroidal body similar to the parent-body of the brachinites in terms of chemical composition, redox conditions, and differentiation history. This is in line with the recent studies of brachinites that included NWA 5400 as "brachinite-like" achondrites (Day et al. 2012; Gardner-Vandy et al. 2013). We interpret the depleted mineral assemblage as representing a restite after partial melting and extraction of silicate melt from a fertile chondritic source rock at ~2 Myr after the start of the solar system. The high concentrations of refractory siderophile elements (Mo, W, and HSE) in the restite require the presence of metal during silicate melt extraction, consistent with the inferred fO_2 of IW-1.21 at magmatic temperatures, as well as the addition of elements to the source rock. This addition of siderophile materials probably happened along with the silicate melt extraction, for example, by fluxing of more oxidized melt (which is enriched in W) through the rock or by addition of later-formed high-S metallic melts. The extraction of the silicate melt most likely marked the peak temperature in the NWA 5363/NWA 5400 assemblage. This is because the main heat-producing isotopes, especially ^{26}Al, were purged with the melt, leaving behind depleted restite rocks. During the following cooling, small amounts of low-degree high-S metal melts formed networks along the equilibrated granular silicate grain boundaries; however, these melts were trapped when the rocks cooled below the Fe-S eutectic and could not efficiently segregate. Thus, while the parent-body of the NWA 5363/NWA 5400 meteorites experienced early silica-saturated magmatism, the heating required to initiate a planetary-wide metal-silicate

fractionation event could not be generated. This suggests that NWA 5363/NWA 5400 derives from a relatively small early-formed asteroidal parent-body, and not from a planetary embryo or planet.

Genetic Relations of NWA 5363/NWA 5400 to Other Planetary Objects

Isotopic anomalies in meteorites are the prime tool to reconstruct genetic relations of planetary materials, because in contrast to elemental signatures or mass-dependent isotope variations, these anomalies are not modified by planetary processes like differentiation, fractional crystallization, or volatile depletion. Thus, isotope anomalies in meteorites provide a direct fingerprint of their bulk parent-body composition. While this genetic fingerprinting was traditionally limited to the use of O isotopes (Clayton 2003), in the last decade a range of other elements were identified to exhibit planetary-scale nucleosynthetic isotope anomalies (Table 3). As the anomalies observed for different elements are often not directly correlated, this allows for multiparameter approaches in planetary genetics, e.g., the testing of genetic relations that were proposed by O isotopes, and multi-isotope minimization models to constrain the origin of planetary building blocks (e.g., Dauphas et al. 2014a).

The terrestrial O isotopic composition reported for NWA 5400 (Irving et al. 2009; Shukolyukov et al. 2010) and NWA 5363 (Larouci et al. 2013) has been used to suggest a close genetic relationship between the nebular reservoirs from which the NWA 5363/NWA 5400 parent-body and the Earth accreted. Our O isotope analyses of NWA 5363/NWA 5400 confirm the terrestrial composition of the NWA 5363/NWA 5400 parent-body. In fact, the NWA 5363/NWA 5400 meteorites are, besides lunar samples (Young et al. 2016), currently the only known extraterrestrial materials with an O isotopic composition identical to the bulk Earth. However, our multi-isotope approach also reveals that in most elements other than O, significant differences exist between the isotopic makeup of NWA 5363/NWA 5400 and the Earth. The Ca, Ti, Cr, Mo, Ru, and Nd isotope data of NWA 5363/NWA 5400 are significantly different from the terrestrial composition, and rather akin to the one of ordinary chondrites (Table 3, Figs. 4 and 5). Taken together, the isotopic compositions of NWA 5363/NWA 5400 cannot be matched by any known meteorite type and supports the classification of these meteorites as ungrouped achondrites. Thus, NWA 5363/NWA 5400 are not direct samples of the terrestrial reservoir. They are neither remnants of the Moon-forming impact nor terrene meteorites sampling the proto-Earth. Instead, they sample a parent-body that accreted from a nebular reservoir isotopically similar to the ones of the ordinary and enstatite chondrites, but markedly different from the source region of the carbonaceous chondrites.

Implications for the Earth-Forming Reservoir and the Composition of the Earth

The Earth is thought to have formed over tens of millions of years by stochastic accretion of planetesimals and planetary embryos originating from various heliocentric distances, with the majority coming from a narrow annulus around 1 AU (O'Brien et al. 2006). Furthermore, correlated Mo and Ru isotope anomalies suggest that the materials of the main phase of Earth's accretion and the late veneer were derived from the same source region (Dauphas et al. 2004; Burkhardt et al. 2011; Fischer-Gödde et al. 2015; Fischer-Gödde and Kleine 2017). This potentially homogeneous source region was dubbed Inner Disk Uniform Reservoir (IDUR) and may have extended up to around 1.5 AU (Dauphas et al. 2014a). Located at ~1.5 AU, Mars, the closest planetary neighbor of the Earth, already exhibits a markedly different isotopic (and elemental) composition (Figs. 3–5), highlighting that the two bodies accreted from a significantly different mix of materials. This implies that the nebular accretion disk must have been heterogeneous at least at the scale sampled by Earth and Mars. Given that most known meteoritic samples derive from the asteroid belt, i.e., beyond the orbit of Mars, it is no surprise that these samples are isotopically distinct from the Earth and cannot be taken as representative of the building blocks of the Earth. However, gravitational perturbations of planetesimals during the growths of planetary embryos and planets may have scattered some of the bodies originally located in the Earth's main accretion region into the asteroid belt (Bottke et al. 2006; Walsh et al. 2012). For example, enstatite chondrites are isotopically very similar to the Earth, while the isotopic and elemental composition of Mars can be regarded as a mixture between enstatite chondrites and ordinary chondrites (Sanloup et al. 1999; Tang and Dauphas 2012). This might indicate that enstatite chondrites sample an isotopic reservoir originally located somewhere in between the orbits of the materials forming the Earth and Mars, and probably contributed to the composition of both planets. If true, this implies that some materials from the terrestrial planet-forming region have ended up in the asteroid belt. If Mars is a mixture between ordinary and enstatite chondrites, then the Earth could be seen as a mixture between enstatite chondrites and an endmember that is not sampled up to now in our collections. Due to the oxidized nature, which would

Table 3. Isotope anomalies of planetary materials. The literature data compilation on which this table is based is provided in Table S1.

	Δ′17O	ε^{48}Ca	ε^{50}Ti	ε^{54}Cr	ε^{62}Ni	ε^{64}Ni	ε^{84}Sr	ε^{96}Zr	ε^{92}Mo	ε^{100}Ru	ε^{135}Ba	ε^{145}Nd	ε^{144}Sm
Chondrites													
Carbonaceous chondrites													
CI	0.07 ± 0.28	2.05 ± 0.20	1.85 ± 0.12	1.56 ± 0.06	0.20 ± 0.14	0.55 ± 0.48	0.40 ± 0.10	0.34 ± 0.24	1.12 ± 0.59	−0.24 ± 0.13	0.27 ± 0.14	−0.21 ± 0.13	−1.02 ± 0.46
CM	−2.52 ± 0.46	±	3.01 ± 0.10	1.02 ± 0.08	0.10 ± 0.03	0.33 ± 0.16	0.40 ± 0.09	0.76 ± 0.37	5.77 ± 1.21	−1.23 ± 1.51	0.34 ± 0.31	0.08 ± 0.06	−0.65 ± 0.66
CO	−4.21 ± 0.68	3.87 ± 0.56	3.77 ± 0.50	0.77 ± 0.33	0.11 ± 0.03	0.26 ± 0.11	0.41 ± 0.21	0.69 ± 0.25	1.95 ± 0.50	−0.92 ± 1.22	±	±	±
CV	−3.99 ± 0.33	3.92 ± 0.50	3.65 ± 0.34	0.87 ± 0.07	0.11 ± 0.03	0.31 ± 0.09	0.63 ± 0.10	1.10 ± 0.31	2.87 ± 0.67	−1.17 ± 0.22	0.26 ± 0.41	0.03 ± 0.05	−0.87 ± 0.17
CK	−3.99 ± 0.33	±	3.63 ± 0.40	0.48 ± 0.30	±	±	±	0.45 ± 0.25	2.16 ± 0.85	−1.10 ± 0.23	±	±	±
CR	−2.02 ± 0.24	±	2.60 ± 0.30	1.31 ± 0.10	0.09 ± 0.05	0.36 ± 0.07	±	1.03 ± 0.40	3.58 ± 0.64	−0.76 ± 0.45	±	±	±
CH	−1.49 ± 0.18	±	±	1.37 ± 0.29	±	0.00 ± 0.00	±	±	±	−0.91 ± 0.13	±	±	±
CB	−2.25 ± 0.10	±	2.04 ± 0.07	1.21 ± 0.09	±	±	±	0.96 ± 0.25	1.74 ± 0.25	−1.04 ± 0.13	±	±	±
Ordinary chondrites													
H	0.67 ± 0.10	−0.24 ± 0.30	−0.64 ± 0.17	−0.36 ± 0.08	−0.06 ± 0.03	−0.17 ± 0.05	−0.13 ± 0.10	0.67 ± 0.44	0.74 ± 0.24	−0.27 ± 0.04	0.08 ± 0.13	0.05 ± 0.03	0.06 ± 0.06
L	0.97 ± 0.09	−1.17 ± 0.68	−0.63 ± 0.08	−0.40 ± 0.10	−0.04 ± 0.03	−0.11 ± 0.03	−0.11 ± 0.21	±	0.76 ± 0.60	−0.28 ± 0.13	0.14 ± 0.04	0.09 ± 0.13	0.02 ± 0.17
LL	1.11 ± 0.11	−0.15 ± 0.39	−0.66 ± 0.14	−0.42 ± 0.07	−0.07 ± 0.03	−0.19 ± 0.06	−0.43 ± 0.10	0.34 ± 0.25	0.87 ± 1.13	0.12 ± 0.70	0.08 ± 0.05	0.06 ± 0.18	0.05 ± 0.23
OC mean	0.92 ± 0.05	−0.41 ± 0.64	−0.64 ± 0.07	−0.39 ± 0.04	−0.06 ± 0.02	−0.16 ± 0.04	−0.17 ± 0.15	0.60 ± 0.35	0.77 ± 0.15	−0.24 ± 0.06	0.10 ± 0.05	0.06 ± 0.03	0.05 ± 0.05
Rumuruti chondrites													
R	2.58 ± 0.20	±	±	0.16 ± 0.50	±	±	±	±	±	−0.39 ± 0.13	±	±	±
Enstatite chondrites													
EH	−0.09 ± 0.12	−0.32 ± 0.56	−0.14 ± 0.07	0.04 ± 0.08	0.03 ± 0.03	0.07 ± 0.08	−0.21 ± 0.12	−0.02 ± 0.30	0.65 ± 1.11	−0.16 ± 0.25	0.17 ± 0.07	0.05 ± 0.03	−0.02 ± 0.13
EL	−0.04 ± 0.08	−0.38 ± 0.26	−0.24 ± 0.21	0.04 ± 0.07	−0.03 ± 0.07	−0.05 ± 0.05	±	±	0.51 ± 0.30	−0.08 ± 0.05	±	0.03 ± 0.04	0.27 ± 0.24
EC mean	−0.06 ± 0.03	−0.37 ± 0.46	−0.18 ± 0.06	0.04 ± 0.05	0.00 ± 0.03	0.01 ± 0.08	−0.21 ± 0.12	−0.02 ± 0.30	0.56 ± 0.43	−0.08 ± 0.03	0.17 ± 0.07	0.04 ± 0.02	0.00 ± 0.08
Achondrites													
Acapulcoites	−1.17 ± 0.13	±	−1.30 ± 0.05	−0.75 ± 0.25	±	±	±	±	±	±	±	±	±
Lodranites	−1.17 ± 0.13	±	±	−0.34 ± 0.25	±	±	±	±	±	±	±	±	±
Brachinites	−0.28 ± 0.15	±	±	±	±	±	±	±	±	±	±	±	±
Winonaites	−0.56 ± 0.08	±	±	±	±	±	±	±	±	±	±	±	±
NWA 5363/ NWA 5400	−0.06 ± 0.07	−0.53 ± 0.20	−1.02 ± 0.10	−0.37 ± 0.13	0.01 ± 0.03	0.04 ± 0.08	±	±	0.53 ± 0.22	−0.34 ± 0.13	±	0.11 ± 0.06	0.27 ± 0.43
Angrites	−0.08 ± 0.06	−1.27 ± 0.15	−1.18 ± 0.08	−0.43 ± 0.15	0.01 ± 0.05	0.00 ± 0.00	0.00 ± 0.10	±	−0.14 ± 0.75	±	±	−0.11 ± 0.26	±
Aubrites	−0.03 ± 0.09	−0.44 ± 0.59	−0.06 ± 0.11	−0.16 ± 0.19	0.05 ± 0.19	0.00 ± 0.00	±	±	±	±	±	±	±
HED	−0.24 ± 0.06	−1.33 ± 0.37	−1.23 ± 0.05	−0.67 ± 0.09	0.03 ± 0.12	0.00 ± 0.00	0.01 ± 0.10	0.47 ± 0.21	±	±	0.05 ± 0.04	0.10 ± 0.04	±
Urelites	−1.30 ± 0.22	−2.00 ± 0.63	−1.85 ± 0.26	−0.92 ± 0.05	−0.05 ± 0.10	0.00 ± 0.00	±	±	±	±	±	±	±
Mars	0.25 ± 0.06	−0.11 ± 0.72	−0.49 ± 0.23	−0.18 ± 0.05	0.04 ± 0.03	±	−0.25 ± 0.15	±	0.20 ± 0.75	±	±	−0.02 ± 0.01	±
Moon	−0.04 ± 0.06	±	−0.03 ± 0.04	0.15 ± 0.10	±	±	−0.22 ± 0.13	±	±	±	±	±	±
Earth	−0.05 ± 0.06	0 ± 0	0 ± 0	0 ± 0	0 ± 0	0 ± 0	0 ± 0	0 ± 0	0 ± 0	0 ± 0	0 ± 0	0 ± 0	0 ± 0
Mesosiderites	−0.25 ±	±	−1.27 ± 0.16	−0.69 ± 0.11	±	±	±	±	±	±	±	±	±
Pallasites													
MG pal	−4.70 ± 0.10	±	−1.37 ± 0.08	−0.39 ± 0.40	±	±	±	±	1.06 ± 0.34	−0.45 ± 0.29	±	±	±
Eagle station Pal	−0.15 ± 0.10	±	±	0.71 ± 0.10	±	±	±	±	1.14 ± 0.24	±	±	±	±
Iron meteorites													
IAB	−0.45 ±	±	±	±	±	±	±	±	−0.12 ± 0.42	−0.06 ± 0.07	±	±	±
IC	±	±	±	±	−0.10 ± 0.12	−0.29 ± 0.20	±	±	0.57 ± 0.31	±	±	±	±
IIAB	−0.61 ±	±	±	±	−0.10 ± 0.09	−0.29 ± 0.10	±	±	1.36 ± 0.70	−0.46 ± 0.05	±	±	±
IIC	±	±	±	±	±	±	±	±	±	±	±	±	±
IID	±	±	±	±	±	±	±	±	1.29 ± 0.64	−0.74 ± 0.48	±	±	±
IIE	0.60 ±	±	±	−0.59 ± 0.13	±	±	±	±	0.71 ± 0.24	±	±	±	±
IIIAB	−0.15 ±	±	±	−0.85 ± 0.06	−0.12 ± 0.02	−0.40 ± 0.14	±	±	1.24 ± 0.64	−0.63 ± 0.06	±	±	±
IIICD	±	±	±	±	±	±	±	±	−0.02 ± 0.62	±	±	±	±
IIIE	±	±	±	±	±	±	±	±	1.11 ± 0.58	±	±	±	±
IIIF	±	±	±	±	±	±	±	±	1.30 ± 1.14	±	±	±	±
IVA	1.15 ±	±	±	±	−0.07 ± 0.05	−0.28 ± 0.21	±	±	0.78 ± 0.28	−0.29 ± 0.09	±	±	±
IVB	±	±	±	±	0.06 ± 0.04	0.13 ± 0.08	±	±	1.91 ± 0.17	−0.90 ± 0.05	±	±	±

Values are presented as mean ± 95% CI.

balance the highly reduced composition of enstatite chondrites, and the terrestrial O isotopic composition, NWA 5363/NWA 5400 would have been a likely candidate for this endmember. However, the observation of ordinary chondrite-like nucleosynthetic Ca, Ti, Cr, Mo, and Ru anomalies in NWA 5363/NWA 5400 does not support this hypothesis. If enstatite chondrites indeed contributed significantly to the makeup of the Earth, then the "missing link" in the genetic description of the Earth would be a sample from a relatively oxidized (~−1 ΔIW) parent-body with high Mg/Si and δ^{30}Si values and an excess in *s*-process Mo, Ru, and Nd as well as slightly positive Δ^{17}O, ε^{48}Ca, and ε^{50}Ti anomalies. A continuous analytical effort to isotopically characterize the ~250 ungrouped meteorites (Meteoritical Bulletin Database) might eventually either identify this material or the terrestrial reservoir, as would samples from Venus or Mercury.

As the terrestrial reservoir is neither sampled by any known meteorite directly, nor can it be reproduced by any combination of known meteorites, care must be taken when using the isotopic composition of chondrites as proxy for the composition of the Earth. This is particularly evident for interpreting (1) stable isotope data with respect to fractionation processes among geochemical reservoirs and (2) radiometric signatures of short-lived nuclides with respect to planetary differentiation.

An example for the first case is the interpretation of the terrestrial and meteoritic Si isotope record. By taking the Mg/Si ratio and mass-dependent silicon isotope composition of ordinary and carbonaceous chondrites as representative of the bulk Earth, it was suggested that the high Mg/Si ratio and δ^{30}Si value of the BSE are the result of partitioning of 8–12 wt% Si in the Earth's core (Georg et al. 2007). However, enstatite chondrites exhibit lower Mg/Si ratios and δ^{30}Si values than ordinary or carbonaceous chondrites, while angrite meteorites exhibit a much higher δ^{30}Si value (Pringle et al. 2014; Dauphas et al. 2015). As the δ^{30}Si and Mg/Si variations in these bodies are unrelated to core formation but rather reflect nebular processes, the composition of the bulk Earth is more uncertain than previously thought, which strongly limits the use of Si isotopes as tracer of Si in the Earth's core. Taking the nebular fractionation trend as additional constraint into account, the range of Si in the core is now estimated to 3.6 (+6.0/−3.6) wt% Si (Dauphas et al. 2015).

An example for the second case is the interpretation of the terrestrial ^{142}Nd rock record. The short-lived ^{146}Sm-^{142}Nd system ($t_{1/2}$ ~103 Ma) is a powerful tool to determine the time scales and processes involved in the early silicate differentiation of the Earth, Moon, and Mars (e.g., Harper and Jacobsen 1992; Harper et al. 1995; Nyquist et al. 1995). However, the inferred ages critically depend on the assumed ^{142}Nd/^{144}Nd and Sm/Nd of the bulk Earth. The ^{142}Nd/^{144}Nd ratio of the modern accessible Earth is slightly higher than those of chondritic meteorites. Assuming a chondritic ^{142}Nd/^{144}Nd for the bulk Earth, this observation is interpreted in chronological terms as evidence for either the formation and sequestration of an early enriched hidden reservoir within a few Ma after the start of the solar system (Boyet and Carlson 2005), or the evolution of the Earth with a superchondritic Sm/Nd (Caro et al. 2008), perhaps resulting from the collisional erosion of early-formed crust (O'Neill and Palme 2008). Both of these interpretations severely change our understanding of the makeup and the evolution of the Earth. However, ^{142}Nd/^{144}Nd seems to be variable among different chondrite groups (with enstatite chondrites being closest to the Earth, followed by ordinary chondrites and carbonaceous chondrites [Gannoun et al. 2011]), and the variations appear to be correlated with anomalies in nonradiogenic Nd isotopes (Burkhardt et al. 2016). This suggests that the ^{142}Nd/^{144}Nd offset between chondrites and the accessible Earth is not of chronological significance, but rather of nucleosynthetic origin. Indeed, after correcting the measured ^{142}Nd/^{144}Nd values for nucleosynthetic effects using the anomalies in the nonradiogenic Nd isotopes, no significant ^{142}Nd/^{144}Nd offset between chondrites and the accessible Earth remains, superseding the need for hidden reservoir of superchondritic Earth models (Burkhardt et al. 2016).

Taken these observations together, the following two simple guidelines of how to use chondrites for estimating the isotopic composition of the bulk Earth can be given.

1. Whenever mass-dependent or mass-independent isotope variations exist among different groups of chondrites, caution should be exercised in assuming that any of the chondrite materials may represent the composition of the Earth. Additional constraints are needed to establish the bulk Earth's isotopic composition. These might be elemental fractionation trends (as in the case of Si) or nucleosynthetic production relations among different isotopes to disentangle radiogenic and nucleosynthetic contributions (as in the case of ^{142}Nd).
2. Vice versa, when all chondrite groups exhibit the same isotope composition for a given element, it is safe to assume that the bulk Earth is also characterized by this chondritic value.

CONCLUSIONS

Our petrographic, chemical, and isotopic investigation of the ungrouped meteorites NWA 5363

and NWA 5400 revealed that they are paired samples from a relatively small and oxidized primitive achondrite parent-body that accreted and partially differentiated within 3 Myr after the start of the solar system. Despite its terrestrial O isotope signature, which was taken as evidence for a potential origin from the Earth-forming inner disk region, the discovery of nucleosynthetic anomalies in Ca, Ti, Cr, Mo, Ru, and Nd reveals that the NWA 5363/NWA 5400 parent-body is not closely related to the Earth. It is thus not the "missing link" in the planetary genetics that could explain the composition of the Earth by the mixing of known meteorites.

Isotopic investigations on the ~250 ungrouped meteorites (Meteoritical Bulletin Database) and samples from Mercury or Venus might eventually identify this missing component and certainly will shed further light on the isotopic makeup of the Earth.

Until this primitive component sampling the terrestrial reservoir is identified, care must be taken when using meteorites to infer the bulk isotopic composition of the Earth, particularly if the isotopic composition of a given element varies among different types of chondrites.

Acknowledgments—This work was supported by a SNF postdoc fellowship (SNF PBE2PZ-145946) (C.B.) and NASA grants (NNX14AK09G, OJ-30381-0036A, NNX15AJ25G) (N.D.). We thank G. Budde for running the spiked samples in Münster, and T. Burbine and Associate Editor M. Caffee for reviews.

Editorial Handling—Dr. Marc Caffee

REFERENCES

Akram W., Schönbächler M., Bisterzo S., and Gallino R. 2015. Zirconium isotope evidence for the heterogeneous distribution of s-process materials in the solar system. *Geochimica et Cosmochimica Acta* 165:484–500.

Allègre C. J., Poirier J.-P., Humler E., and Hofmann A. W. 1995. The chemical composition of the Earth. *Earth and Planetary Science Letters* 134:515–526.

Amelin Y. and Irving A. J. 2011. U-Pb systematics of the ultramafic achondrite Northwest Africa 5400 (abstract #5197). *Meteoritics & Planetary Science* 46:A10.

Andreasen R. and Sharma M. 2007. Mixing and homogenization in the early solar system: Clues from Sr, Ba, Nd, and Sm isotopes in meteorites. *Astrophysical Journal* 665:874.

Borg L. E., Brennecka G. A., and Symes S. J. K. 2016. Accretion timescale and impact history of Mars deduced from the isotopic systematics of Martian meteorites. *Geochimica et Cosmochimica Acta* 175:150–167.

Bottke W. F., Nesvorny D., Grimm R. E., Morbidelli A., and O'Brien D. P. 2006. Iron meteorites as remnants of planetesimals formed in the terrestrial planet region. *Nature* 439:821–824.

Boyet M. and Carlson R. W. 2005. ^{142}Nd evidence for early (>4.53 Ga) global differentiation of the silicate Earth. *Science* 309:576–581.

Brey G. P. and Köhler T. 1990. Geothermobarometry in four-phase lherzolites II. New thermobarometers, and practical assessment of existing thermobarometers. *Journal of Petrology* 31:1353–1378.

Budde G., Burkhardt C., Fischer-Gödde M., Kruijer T. S., and Kleine T. 2016. Molybdenum isotopic evidence for the origin of chondrules and a distinct genetic heritage of carbonaceous and non-carbonaceous meteorites. *Earth and Planetary Science Letters* 454:293–303.

Burkhardt C., Kleine T., Oberli F., Pack A., Bourdon B., and Wieler R. 2011. Molybdenum isotope anomalies in meteorites: Constraints on solar nebula evolution and origin of the Earth. *Earth and Planetary Science Letters* 312:390–400.

Burkhardt C., Hin R. C., Kleine T., and Bourdon B. 2014. Evidence for Mo isotope fractionation in the solar nebula and during planetary differentiation. *Earth and Planetary Science Letters* 391:201–211.

Burkhardt C., Borg L. E., Brennecka G. A., Shollenberger Q. R., Dauphas N., and Kleine T. 2016. A nucleosynthetic origin for the Earth's anomalous ^{142}Nd composition. *Nature* 537:394–398.

Carignan J., Hild P., Morel J., and Yeghicheyan D. 2001. Routine analysis of trace elements in geochemical samples using flow injection and low-pressure on-line liquid chromatography coupled to ICP-MS: A study of geochemical references materials BR, DR-N, UB-N, AN-G and GH. *Geostandard Newsletter* 25:187–198.

Carlson R. W., Boyet M., and Horan M. 2007. Chondrite barium, neodymium, and samarium isotopic heterogeneity and early Earth differentiation. *Science* 316:1175–1178.

Caro G., Bourdon B., Halliday A. N., and Quitté G. 2008. Super-chondritic Sm/Nd ratios in Mars, the Earth and the Moon. *Nature* 452:336–339.

Chen J., Papanastassiou D., and Wasserburg G. 2010. Ruthenium endemic isotope effects in chondrites and differentiated meteorites. *Geochimica et Cosmochimica Acta* 74:3851–3862.

Chen H. W., Lee T., Lee D. C., Shen J. J., and Chen J. C. 2011. ^{48}Ca heterogeneity in differentiated meteorites. *The Astrophysical Journal Letters* 743:L23.

Clayton R. N. 2003. Oxygen isotopes in meteorites. In *Meteorites, comets, and planets*, edited by Davis A. M. Treatise on Geochemistry, vol. 1. Oxford, UK: Elsevier-Pergamon. pp. 129–142.

Dauphas N. 2017. The isotopic nature of Earth's accreting materials. *Nature* 542. doi:10.1038/nature20830

Dauphas N., Marty B., and Reisberg L. 2002. Molybdenum evidence for inherited planetary scale isotope heterogeneity of the protosolar nebula. *Astrophysical Journal* 565:640.

Dauphas N., Davis A. M., Marty B., and Reisberg L. 2004. The cosmic molybdenum-ruthenium isotope correlation. *Earth and Planetary Science Letters* 226:465–475.

Dauphas N., Chen J. H., Zhang J., Papanastassiou D. A., Davis A. M., and Travaglio C. 2014a. Calcium-48 isotopic anomalies in bulk chondrites and achondrites: Evidence for a uniform isotopic reservoir in the inner protoplanetary disk. *Earth and Planetary Science Letters* 407:96–108.

Dauphas N., Burkhardt C., Warren P. H., and Fang-Zhen T. 2014b. Geochemical arguments for an Earth-like Moon-

forming impactor. *Philosophical Transactions of the Royal Society of London. A* 372:20130244.

Dauphas N., Poitrasson F., Burkhardt C., Kobayashi H., and Kurosawa K. 2015. Planetary and meteoritic Mg/Si and δ^{30}Si variations inherited from solar nebula chemistry. *Earth and Planetary Science Letters* 427:236–248.

Day J. M. D., Ash R. D., Liu Y., Bellucci J. J., Rumble D. I. I. I., McDonough W. F., Walker R. J., and Taylor L. A. 2009. Early formation of evolved asteroidal crust. *Nature* 457:179–182.

Day J. M. D., Walker R. J., Ash R. D., Liu Y., Rumble D., Irving A. J., Goodrich C. A., Tait K., McDonough W. F., and Taylor L. A. 2012. Origin of felsic achondrites Graves Nunataks 06128 and 06129, and ultramafic brachinites and brachinite-like achondrites by partial melting of volatile-rich primitive parent bodies. *Geochimica et Cosmochimica Acta* 81:94–128.

Fischer-Gödde M. and Kleine T. 2017. Ruthenium isotopic evidence for an inner solar system origin of the late veneer. *Nature*, doi:10.1038/nature21045.

Fischer-Gödde M., Burkhardt C., Kruijer T., and Kleine T. 2015. Ru isotope heterogeneity in the solar protoplanetary disk. *Geochimica et Cosmochimica Acta* 168:151–171.

Gannoun A., Boyet M., Rizo H., and El Goresy A. 2011. ^{146}Sm-^{142}Nd systematics measured in enstatite chondrites reveals a heterogeneous distribution of ^{142}Nd in the solar nebula. *Proceedings of the National Academy of Sciences* 108:7693–7697.

Gardner-Vandy K. G., Lauretta D. S., and McCoy T. J. 2013. A petrologic, thermodynamic and experimental study of brachinites: Partial melt residues of an R chondrite-like precursor. *Geochimica et Cosmochimica Acta* 122:36–57.

Garvie L. A. J. 2012. Meteoritical Bulletin No. 99. *Meteoritics & Planetary Science* 47:E1–E52.

Georg R. B., Halliday A. N., Schauble E. A., and Reynolds B. C. 2007. Silicon in the Earth's core. *Nature* 447:1102–1106.

Goldschmidt V. M. 1929. The distribution of the chemical elements. *Proceedings of the Royal Institution of Great Britain* 26:73–86.

Göpel C. and Birck J. L. 2010. Mn/Cr systematics: A tool to discriminate the origin of primitive meteorites. Goldschmidt Conference. p. 348.

Göpel C., Birck J. L., Galy A., Barrat J. A., and Zanda B. 2015. Mn–Cr systematics in primitive meteorites: Insights from mineral separation and partial dissolution. *Geochimica et Cosmochimica Acta* 156:1–24.

Harper C. L. and Jacobsen S. B. 1992. Evidence from coupled ^{147}Sm-^{143}Nd and ^{146}Sm-^{142}Nd systematics for very early (4.5 Gyr) differentiation of the Earth's mantle. *Nature* 360:728–732.

Harper C. L., Nyquist L. E., Bansal B., Wiesmann H., and Shih C. Y. 1995. Rapid accretion and early differentiation of Mars indicated by ^{142}Nd/^{144}Nd in SNC meteorites. *Science* 267:213–217.

Herwartz D., Pack A., Friedrichs B., and Bischoff A. 2014. Identification of the giant impactor Theia in lunar rocks. *Science* 344:1146–1150.

Irving A. J., Rumble D., Kuehner S. M., Gellissen M., and Hupe G. M. 2009. Ultramafic achondrite Northwest Africa 5400: A unique brachinite-like meteorite with terrestrial oxygen isotopic composition (abstract #2332). 40th Lunar and Planetary Science Conference. CD-ROM.

Jarosewich E. 1990. Chemical analyses of meteorites: A compilation of stony and iron meteorite analyses. *Meteoritics* 25:323–337.

Jarosewich E., Clarke R. S., and Barrows J. N. 1987. The Allende Meteorite reference sample. *Smithsonian Contributions of the Earth Sciences* 27:49.

Kleine T., Mezger K., Münker C., Palme H., and Bischoff A. 2004. 182Hf-182W isotope systematics of chondrites, eucrites, and Martian meteorites: Chronology of core formation and early mantle differentiation in Vesta and Mars. *Geochimica et Cosmochimica Acta* 68:2935–2946.

Kleine T., Touboul M., Bourdon B., Nimmo F., Mezger K., Palme H., Jacobsen S. B., Yin Q.-Z., and Halliday A. N. 2009. Hf-W chronology of the accretion and early evolution of asteroids and terrestrial planets. *Geochimica et Cosmochimica Acta* 73:5150–5188.

Kleine T., Hans U., Irving A. J., and Bourdon B. 2012. Chronology of the angrite parent body and implications for core formation in protoplanets. *Geochimica et Cosmochimica Acta* 84:186–203.

Köhler T. P. and Brey G. 1990. Calcium exchange between olivine and clinopyroxene calibrated as a geothermobarometer for natural peridotites from 2 to 60 kb with applications. *Geochimica et Cosmochimica Acta* 54:2375–2388.

Kruijer T. S., Kleine T., Fischer-Gödde M., Burkhardt C., and Wieler R. 2014. Nucleosynthetic W isotope anomalies and the Hf–W chronometry of Ca–Al-rich inclusions. *Earth and Planetary Science Letters* 403:317–327.

Larouci N., Jambon A., Chennaoui Aoudjehane H., Boudouma O., Gattacceca J., and Sonzogni C. 2013. NWA 5363: Remnants of a terrestrial embryo? (abstract #5185). 76th Annual Meteoritical Society Meeting Meteoritics & Planetary Science 48.

Larsen K. K., Trinquier A., Paton C., Schiller M., Wielandt D., Ivanova M. A., Connelly J. N., Norlund A., Krot A. N., and Bizzarro M. 2011. Evidence for magnesium isotope heterogeneity in the solar protoplanetary disk. *The Astrophysical Journal Letters* 735:L37.

Millet M.-A. and Dauphas N. 2014. Ultra-precise titanium stable isotope measurements by double-spike high resolution MC-ICP-MS. *Journal of Analytical Atomic Spectrometry* 29:1444–1458.

Moynier F., Day J. M., Okui W., Yokoyama T., Bouvier A., Walker R. J., and Podosek F. A. 2012. Planetary-scale strontium isotopic heterogeneity and the age of volatile depletion of early solar system materials. *Astrophysical Journal* 758:45.

Nyquist L. E., Wiesmann H., Bansal B., Shih C. Y., Keith J. E., and Harper C. L. 1995. ^{146}Sm-^{142}Nd formation interval for the lunar mantle. *Geochimica et Cosmochimica Acta* 59:2817–2837.

O'Brien D. P., Morbidelli A., and Levison H. F. 2006. Terrestrial planet formation with strong dynamical friction. *Icarus* 184:39–58.

O'Neill H. S. C. and Palme H. 2008. Collisional erosion and the non-chondritic composition of the terrestrial planets. *Philosophical Transactions of the Royal Society of London A* 366:4205–4238.

Pack A. and Herwartz D. 2014. The triple oxygen isotope composition of the Earth mantle and understanding δ^{17}O variations in terrestrial rocks and minerals. *Earth and Planetary Science Letters* 390:138–145.

Pack A., Tanaka R., Hering M., Sengupta S., Peters S., and Nakamura E. 2016. The oxygen isotope composition of San Carlos olivine on VSMOW2-SLAP2 scale. *Rapid Communications in Mass Spectrometry* 30:1495–1504.

Palme H. and O'Neill H. S. C. 2014. Cosmochemical estimates of mantle composition. *The mantle and the core*, edited by Carlson R. W. Treatise on Geochemistry, Vol. 3. Oxford: Elsevier-Pergamon. pp. 1–39.

Pravdivtseva O., Meshik A., Hohenberg C. M., and Irving A. J. 2015. I-Xe systematics of brachinite-like ultramafic achondrite Northwest Africa 5400 (abstract #5387). 78th Meeting of the Meteoritical Society Meteoritics & Planetary Science 50.

Pringle E. A., Moynier F., Savage P. S., Badro J., and Barrat J. A. 2014. Silicon isotopes in angrites and volatile loss in planetesimals. *Proceedings of the National Academy of Sciences* 111:17,029–17,032.

Qin L., Alexander C. M. O'D., Carlson R. W., Horan M. F., and Yokoyama T. 2010. Contributors to chromium isotope variation of meteorites. *Geochimica et Cosmochimica Acta* 74:1122–1145.

Regelous M., Elliott T., and Coath C. D. 2008. Nickel isotope heterogeneity in the early solar system. *Earth and Planetary Science Letters* 272:330–338.

Render J., Fischer-Gödde M., Burkhardt C., and Kleine T. 2016. Molybdenum isotopes and the building blocks of the Earth (abstract #2639). 47th Lunar and Planetary Science Conference. CD-ROM.

Robie R. A. and Hemingway B. S. 1995. Thermodynamic properties of minerals and related substances at 298.15 K and 1 bar (10ˆ5 Pascals) pressure and at higher temperatures. *US Geological Survey Bulletin* 2131:461.

Russell H. N. 1941. The cosmical abundance of the elements. *Science* 94:375–381.

Sack R. O. and Ghiorso M. S. 1991. Chromian spinels as petrogenetic indicators: Thermodynamics and petrological applications. *American Mineralogist* 76:827–847.

Sanborn M. E., Carlson R. W., and Wadhwa M. 2015. ^{147,146}Sm–^{143,142}Nd, ^{176}Lu–^{176}Hf, and ^{87}Rb–^{87}Sr systematics in the angrites: Implications for chronology and processes on the angrite parent body. *Geochimica et Cosmochimica Acta* 171:80–99.

Sanborn M. E., Yin Q.-Z., Schmitz B., and Amelin Y. 2016. Northwest Africa 5400/6077: Deciphering the origin of the mysterious achondrite with a new look at the isotopic composition (abstract #2309). 47th Lunar and Planetary Science Conference. CD-ROM.

Sanloup C., Jambon A., and Gillet P. 1999. A simple chondritic model of Mars. *Physics of the Earth and Planetary Interiors* 112:43–54.

Schiller M., Van Kooten E., Holst J. C., Olsen M. B., and Bizzarro M. 2014. Precise measurement of chromium isotopes by MC-ICPMS. *Journal of Analytical Atomic Spectrometry* 29:1406–1416.

Sharp Z. D. 1990. A laser-based microanalytical technique for in situ determination of oxygen isotope ratios of silicates and oxides. *Geochimica et Cosmochimica Acta* 54:1353–1357.

Shukolyukov A. and Lugmair G. W. 2006. Manganese–chromium isotope systematics of carbonaceous chondrites. *Earth and Planetary Science Letters* 250:200–213.

Shukolyukov A., Lugmair G. W., and Irving A. J. 2009. Mn-Cr isotope systematics of angrite northwest Africa 4801 (abstract #1381). 40th Lunar and Planetary Science Conference. CD-ROM.

Shukolyukov A., Lugmair G., Day J. M. D., Walker R. J., Rumble D. III, Nakashima D., Nagao K., and Irving A. J. 2010. Constraints on the formation age, highly siderophile element budget and noble gas isotope compositions of Northwest Africa 5400: An ultramafic achondrite with terrestrial isotope characteristics (abstract #1492). 41st Lunar and Planetary Science Conference. CD-ROM.

Steele R. C. J., Elliott T., Coath C. D., and Regelous M. 2011. Confirmation of mass-independent Ni isotopic variability in iron meteorites. *Geochimica et Cosmochimica Acta* 75:7906–7925.

Stracke A., Palme H., Gellissen M., Münker C., Kleine T., Birbaum K., Günther D., Bourdon B., and Zipfel J. 2012. Refractory element fractionation in the Allende meteorite: Implications for solar nebula condensation and the chondritic composition of planetary bodies. *Geochimica et Cosmochimica Acta* 85:114–141.

Tang H. and Dauphas N. 2012. Abundance, distribution, and origin of ^{60}Fe in the solar protoplanetary disk. *Earth and Planetary Science Letters* 359–360:248–263.

Tang H. and Dauphas N. 2014. ^{60}Fe-^{60}Ni chronology of core formation on Mars. *Earth and Planetary Science Letters* 390:264–274.

Trinquier A., Birck J. L., and Allègre C. J. 2007. Widespread ^{54}Cr heterogeneity in the inner solar system. *Astrophysical Journal* 655:1179.

Trinquier A., Elliott T., Ulfbeck D., Coath C., Krot A. N., and Bizzarro M. 2009. Origin of nucleosynthetic isotope heterogeneity in the solar protoplanetary disk. *Science* 324:374–376.

Usui T., Jones J. H., and Mittlefehldt D. W. 2015. A partial melting study of an ordinary (H) chondrite composition with application to the unique achondrite Graves Nunataks 06128 and 06129. *Meteoritics & Planetary Science* 50:759–781.

Vockenhuber C., Oberli F., Bichler M., Ahmad I., Quitte′ G., Meier M., Halliday A. N., Lee D. C., Kutschera W., Steier P., Gehrke R. J., and Helmer R. G. 2004. New half-life measurement of 182Hf: Improved chronometer for the early solar system. *Physical Review Letters* 93:172501.

Wadhwa M., Shukolyukov A., and Lugmair G. W. 1998. ^{53}Mn–^{53}Cr systematics in Brachina: A record of one of the earliest phases of igneous activity on an asteroid (abstract #1480). 29th Lunar and Planetary Science Conference. CD-ROM.

Walsh K. J., Morbidelli A., Raymond S. N., O'Brien D. P., and Mandell A. M. 2012. Populating the asteroid belt from two parent source regions due to the migration of giant planets—"The Grand Tack." *Meteoritics & Planetary Science* 47:1941–1947.

Warren P. H. and Kallemeyn G. W. 1989. Allan Hills 84025: The second brachinite, far more differentiated than Brachina, and an ultramafic achondrite clast from L chondrite Yamato 75097. Proceedings, 19th Lunar and Planetary Science Conference. pp. 475–486.

Weisberg M. K., Smith C., Benedix G., Herd C. D. K., Righter K., Haack H., Yamaguchi A., Chennaoui Aoudjehane H., and Grossman J. N. 2009. The Meteoritical Bulletin No. 96. *Meteoritics & Planetary Science* 44:1355–1397.

Yamakawa A., Yamashita K., Makishima A., and Nakamura E. 2010. Chromium isotope systematics of achondrites:

Chronology and isotopic heterogeneity of the inner solar system bodies. *The Astrophysical Journal* 720:150.
Young E. D., Kohl I. E., Warren P. H., Rubie D. C., Jacobson S. A., and Morbidelli A. 2016. Oxygen isotopic evidence for vigorous mixing during the Moon-forming giant impact. *Science* 351:493–496.
Zhang J., Dauphas N., Davis A. M., and Pourmand A. 2011. A new method for MC-ICPMS measurement of Ti isotopic composition: Identification of correlated isotope anomalies in meteorites. *Journal of Analytical Atomic Spectrometry* 26:2197–2205.
Zhang J., Dauphas N., Davis A. M., Leya I., and Fedkin A. 2012. The proto-Earth as a significant source of lunar material. *Nature Geoscience* 5:251–255.

SUPPORTING INFORMATION

Additional supporting information may be found in the online version of this article:

Table S1. Full O, Ca, Ti, Cr, Ni, Mo, Ru and W isotope data of Allende, Allegan, Pillistfer, NWA 5363, NWA 5400.

Data S1. Nucleosynthetic anomalies in planetary materials (compilation by C. Burkhardt, 2017).